DTU Library

Cost–benefit analysis and design optimization of wind propulsion systems for a Tanker retrofit case

Reche-Vilanova, M.; Bingham, H. B.; Fluck, M.; Morris, D.; Psaraftis, H. N.

Link back to DTU Orbit

Full length article

Cost–benefit analysis and design optimization of wind propulsion systems for a Tanker retrofit case

M. Reche-Vilanova [a,b] [iD],*, H.B. Bingham [b] [iD], M. Fluck [c], D. Morris [a], H.N. Psaraftis [b] [iD]

[a] *North Windships, Copenhagen, 2450, Denmark*
[b] *Technical University of Denmark, Kongens Lyngby, 2800, Denmark*
[c] *WISAMO - Michelin, Vannes, 56000, France*

ARTICLE INFO

ABSTRACT

This study introduces WindWise, a cost–benefit analysis and design optimization tool for Wind Propulsion Systems (WPS) in sustainable shipping. By integrating route simulations, ship constraints, and fuel pricing scenarios, WindWise determines the optimal WPS configuration to maximize fuel savings and minimize payback periods. A retrofit case study of an oil tanker evaluates two WPS classes—DynaRigs and Rotor Sails—across multiple operational and economic conditions. Results reveal that optimal configurations vary based on constraints: in an unconstrained scenario, larger, well-spaced installations minimize aerodynamic losses, whereas realistic constraints shift the preference towards smaller, distributed setups to mitigate cargo loss and air draft penalties. Rotor Sails offer lower upfront costs and shorter payback periods for modest savings targets and for side-wind routes, while DynaRigs emerge as the more viable solution for higher emissions reductions and long-term profitability. Optimization of WPS configurations proves crucial, with non-optimized configurations exhibiting payback periods over 150% higher than optimized ones. Although payback period remains an important metric, considering both payback and net present value provides a more comprehensive assessment of WPS financial viability, with Rotor Sails generally offering faster payback but DynaRigs delivering higher long-term profitability across most scenarios.

1. Introduction

The International Maritime Organization's (IMO) strategic goals for greenhouse gas (GHG) reduction (MEPC, 2023), along with regulatory incentives like EEDI, EEXI, and CII, have spurred interest in wind propulsion systems (WPS) as sustainable propulsion alternatives. This growing interest is evidenced by the increasing number of WPS installations (Laursen et al., 2023).

Despite this progress, the widespread adoption of WPS remains challenging. Nelissen et al. (2016) identified key barriers to WPS uptake, including applicability to specific ships, cost-efficiency, certainty of performance, and access to capital. Additionally, limited and case-specific performance data, coupled with skepticism in the maritime sector, further hinder adoption. The operation of WPS-equipped ships differs significantly from conventional vessels (Reche-Vilanova et al., 2024a), and potential buyers often struggle to trust or interpret the available information. This challenge is exacerbated by the numerous variables affecting WPS performance, such as ship type, route, WPS class, configuration, deck arrangement, and operational constraints. Without detailed, case-specific performance assessments, skepticism and uncertainty will continue to delay industry confidence and adoption.

Addressing these barriers is critical. Performance Prediction Programs (PPPs) have been developed to evaluate WPS fuel savings and emissions reductions, aiming to provide relevant insights. Early efforts, such as Schenzle (1980) and Bradbury (1980), explored Dynarigs and Rigid sails, while Bordogna (2020) and Van der Kolk (2020) used experimental testing to predict performance for Rotor sails and Dynarigs, including aerodynamic interaction effects. Reche-Vilanova et al. (2021) proposed a generic tool for evaluating performance across various WPS classes. However, while these studies advanced understanding, most PPPs lack robust economic analysis and fail to identify the optimal WPS configuration for specific vessels and operational scenarios.

Recent works have begun addressing these gaps. ShipClean (Tillig and Ringsberg, 2020) evaluated payback periods for predefined WPS designs but relied on user-provided inputs, limiting ideal configuration identification. SEAMAN Winds (Gerhardt et al., 2021) introduced a systematic methodology for assessing WPS benefits at the concept stage, validated through full-scale trials. However, both ShipClean and SEAMAN Winds limit their economic analysis to payback periods, overlooking investment scale and failing to provide a comprehensive financial assessment. Moreover, these tools lack automated optimization methodologies to identify the optimal WPS type, configuration, and arrangement for specific ships, routes, and emission reduction targets. Comparative analyses must also ensure that optimized WPS designs are assessed against other optimized counterparts rather than suboptimal alternatives to ensure fair and accurate evaluations.

This research presents WindWise, an advanced cost–benefit analysis and design optimization tool aimed at facilitating WPS adoption in the shipping sector by addressing key barriers. WindWise identifies the optimal WPS class, configuration, deck arrangement, and position for a given vessel, route, fuel cost scenario, and emissions reduction ambition. It provides an integrated framework to maximize wind potential, reduce operator costs, and enhance industry confidence through improved knowledge and insights. The tool also highlights the strengths and weaknesses of different solutions, supporting informed decision-making and unlocking the full potential of wind propulsion technologies to accelerate the green transition.

The remainder of this paper is organized as follows: Section 2 introduces WindWise and its workflow. Section 3 details the ship model, incorporating all forces and moments exerted by WPS. Section 4 presents the PPP developed for WPS performance prediction. Section 5 describes the route and weather model for predicting sailing conditions. Section 6 outlines the cost model for the economic evaluation of WPS. Section 7 discusses the optimization framework, including objectives, constraints, and limitations. Section 8 validates the model against sea trial data. Section 9 presents the results of the Tanker retrofit case study. Finally, Section 10 concludes the study and proposes future work.

2. WindWise: a Cost–Benefit Analysis Tool for Wind Propulsion Systems optimization

WindWise, the developed Cost–Benefit Analysis Tool for Wind Propulsion Systems (WPS), employs a modular framework, enabling the approximation of unknown data through generic models while seamlessly integrating detailed, case-specific data when available. This adaptability ensures that the tool is suitable for various stages of WPS development, from initial concept evaluation to detailed optimization and implementation.

WindWise also advances the capabilities of the actual North Design Suite of North Windships, enhancing its ability to accurately model and optimize WPS installations. In this paper, we focus on describing and applying the generic models developed within WindWise, particularly for cases where detailed ship and WPS data are unavailable. These generic models provide robust performance and business-case predictions, with accuracy improving as more specific data becomes available.

WindWise is divided into 5 main parts:

- The *Ship Model*: comprising all the hydrodynamic, aerodynamic, and propulsive forces and moments exerted on the Windship through the *Hydro Model*, the *Aero Model*, and the *Engine and Propeller Model*, respectively.
- The *PPP Model*: The Performance Prediction Program (PPP) builds on the existing North Velocity Prediction Program (VPP) to enhance performance predictions of the Windship under various wind and operating conditions.
- The *Route and Weather Model*: simulating the shortest route between two points (departure point A to arrival point B), incorporating historical wind probability distributions along the generated route or for an established average wind condition, and estimating the required sailing time.
- The *Cost Model*: calculating the predicted capital expenditure (CAPEX) for the WPS installation and the corresponding operational expenditure (OPEX) savings achieved through fuel and pollutant emissions reductions for various fuel and market-based measure scenarios.
- The *Optimizer*: Identifying the optimal WPS configuration based on predefined objective functions, such as maximizing fuel savings or minimizing the payback period, while adhering to constraints like maximum air draft or feasible deck placement.

The tool operates as follows: The user provides generic input data, including the ship's characteristics (hull, rudder, propeller, and engine), operational constraints, specific costs, the target Wind Propulsion System (WPS) class for optimization, and the configuration limits for the selected WPS. If some input data are unknown, the tool approximates the values following analytical or semi-empirical approaches or own developed models. Subsequently, all components of the *Ship Model* are initialized. These components collectively calculate the surge and sway forces, as well as the heel and yaw moments, for each respective Windship component. Only these forces and moments are included because the simulations are limited to 4 degrees of freedom (DoF): surge, sway, roll, and yaw.

The *Aero Model* computes the aerodynamic forces and moments exerted by the simulated WPS configuration, accounting for aerodynamic interaction effects, across a wide range of sail trims, wind conditions, and heel angles. The *Hydro Model* evaluates the hydrodynamic forces and moments for various ship speeds, leeway, heel, and rudder angles. The *Engine and Propeller Model*
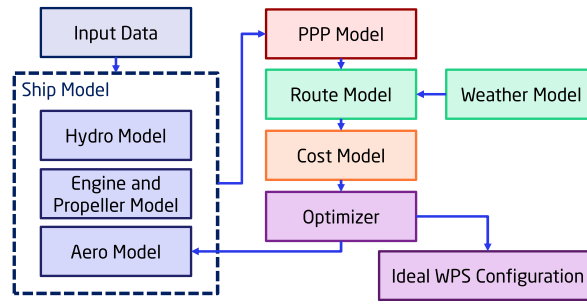
Fig. 1. Schematic outline of WindWise, the Cost–Benefit Analysis and Design Optimization Tool for WPS installations.
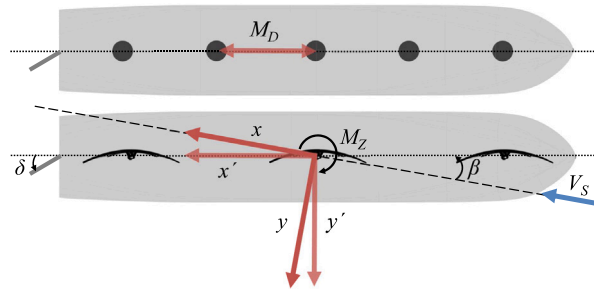

Fig. 2. WindWise coordinate systems and example of a longitudinal WPS arrangement with DynaRigs and Rotor Sails.

determines the forces, moments, and engine power requirements for different ship speeds, incorporating variations in propulsive efficiency.

All these forces and moments are combined as generated force and moment surfaces in the *PPP Model*, which predicts the theoretical sailing performance of the Windship by balancing all the forces and moments while optimizing the independent sail trim to determine the required engine power under various wind conditions. The results feed into the *Route and Weather Model*, which computes the shortest route between two points and predicts the annual-average wind conditions at the waypoints. This model's output estimates the predicted fuel savings for the given scenario, which is then input into the *Cost Model* to calculate the payback period (PBP) and net present value (NPV) of the WPS installation, factoring in CAPEX and OPEX.

Finally, the *Optimizer* identifies the optimal WPS configuration that maximizes fuel savings and minimizes costs. The optimizer adjusts the WPS configuration using the *Aero Model* and iterates through the pipeline until convergence is achieved, delivering a final design recommendation. Fig. 1 provides a schematic overview of WindWise.

The WPS classes currently included in WindWise are DynaRigs, Rotor Sails, single, double, and triple-element Rigid Sails, Turbo Sails, and inflatable single-element sails. Due to its modularity, the tool can model any new WPS design provided its performance coefficients are supplied. WindWise can evaluate multiple WPS configurations at computational speeds comparable to analytical and semi-empirical methods, while achieving significantly enhanced accuracy by leveraging the comprehensive CFD database embedded in the *Aero Model* for passive systems like DynaRigs and Rigid Sails.

This study focuses on evaluating WindWise's performance and providing optimized configurations for two distinct WPS classes: the DynaRig and the Rotor Sail for a real retrofit tanker case. These represent a passive and an active system, respectively, already proven and installed.

The following sections provide detailed descriptions of the methods employed or developed for each model.

2.1. Coordinate system

WindWise employs two distinct coordinate systems: a flow-oriented system fixed to the course through water (x, y, z) and a hull-fixed system (x', y', z'). The origin of both coordinate systems is located at midship on the waterline. Fig. 2 illustrates both coordinate systems, along with the definitions of the leeway and rudder deflection angles, as well as the yaw moment. All forces in the *Ship Model* are computed in the flow-oriented coordinate system, while the hull-fixed system is used in the *PPP Model* to assess overall ship performance. Fig. 2 also illustrates an example of a WPS longitudinal arrangement featuring DynaRigs and Rotor Sails, highlighting the mast distance ratio M_D, defined as the absolute longitudinal spacing between units normalized by the maximum chord length of the WPS under study.

Table 1
WindWise physical effects and limitations.

Group	Effects Included	Effects Neglected
PPPSolver	- Surge and Sway - Roll and Yaw - Steady-state - Minimum engine power or maximum sailing speed	- Sinkage and Trim
Hydro	- Calm deep water resistance - Drift forces - Rudder forces - Hull–rudder interactions - Hull–propeller interactions - WPS weight - Heel angle - Appendage forces	- Heel and drift coupling effects - Shallow water effects - Unsteady ship motions - Sinkage and trim - Added resistance due to ocean waves - Hull-appendages interactions - Drift effects on the rudder and propeller
Aero	- WPSu interactions - WPS-hull interactions - Independent sail trim optimization - Height variation in wind speed - WPS weight - Heel angle - Variations of area, units, and deck arrangement - Longitudinal arrangement - Power required	- WPS-superstructure interactions - Height variation in wind direction - Unsteady WPS aerodynamic performance - Aerodynamic damping of ship motion - Aspect ratio variations - Side-by-side arrangement - Superstructure and hull windage
Propulsion	- Propeller efficiency variation - Main Engine efficiency variation - Propeller type	- Auxiliary engine performance
Operation	- Operating limits - Constant sailing speed - Constant shaft speed - Hindcast weather data	- Idle time - Maneuvering in harbors - Route optimization
Costs	- WPS CAPEX - Fuel savings - Emissions savings - Maintenance costs - Cost of cargo space lost - IMO Indexes calculations	- Crew training costs - Life cycle assessment
Optimizer	- Maximum Air draft - Feasible Deck Placement	- Vibrations and Noise

2.2. Physical effects and limitations

The physical effects included or neglected in WindWise are summarized in Table 1, with further details provided in the respective sections of this article detailing each of the models. While these simplifications may have real-world implications, they are considered appropriate for the study's objective, which focuses on modeling the primary operational differences between conventional and WPS-equipped vessels to reduce model complexity.

3. Ship model

The *Ship Model* integrates all hydrodynamic, aerodynamic, and propulsive forces and moments acting on the ship. These forces and moments are categorized into four distinct models: the *Hydro Model*, the *Aero Model*, and the *Engine and Propeller Model*. Together, they contribute to the total surge force F_X, sway force F_Y, heel moment M_X, and yaw moment M_Z, defined as,

$$F_X = X_H + X_R + X_A + X_W + X_P, \tag{1}$$

$$F_Y = Y_H + Y_R + Y_A + Y_W, \tag{2}$$

$$M_X = M_H + Y_H v_H + Y_R v_R + Y_A v_A + Y_W v_W, \tag{3}$$

$$M_Z = Y_H l_H + Y_R l_R + Y_A l_A + Y_W l_W, \tag{4}$$

where X represents the surge force components of each model, while Y corresponds to the sway force components. M_H stands for the hull righting moment, while l and v denote the longitudinal and vertical centers of effort, respectively, all calculated relative to the coordinate origin. The subindex nomenclature used for each of the force and center of effort components is defined as follows,
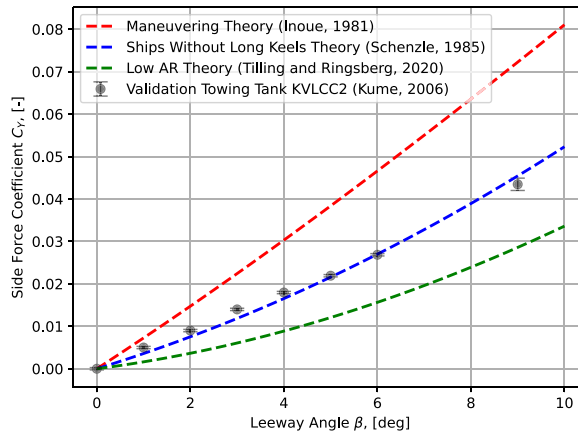
• H: Bare hull components

Fig. 3. Non-dimensional hydrodynamic side force coefficient for the KVLCC2 as function of leeway angle for different predictive approaches and towing tank data.

- *R*: Rudder components
- *A*: Appendage components
- *W*: Wind Propulsion System components
- *P*: Propeller components

Each section below provides a detailed explanation of these forces, moments, and their respective centers of effort for each individual model. The last section details the model limitations.

3.1. Hydro Model

The *Hydro Model* computes forces and moments on the hull, rudder(s), and appendages (if applicable) under typical Windship operating conditions, characterized by non-zero heel and leeway angles. The model is structured into three primary components: the hull, the rudder, and the appendages, each with distinct force and moment estimation methodologies. Detailed formulations for each method are provided in the subsequent subsections.

3.1.1. Hull model

This approach estimates the hydrostatics and hydrodynamic forces and moments using established analytical and semi-empirical methods. The calm deep water resistance as a function of speed is calculated following the method proposed by Hollenbach (1998), where the total calm water resistance X_{CW} is calculated following,

$$X_{CW} = C_R \frac{\rho_w}{2} V^2 BT + C_{FR} \frac{\rho_w}{2} V^2 S_W, \tag{5}$$

where C_R and C_{FR} are the non-dimensional residual and frictional resistance coefficients, respectively. ρ_w is the water density, V is the ship speed, B is the ship beam, T is the ship draft, and S_W is the wetted surface.

To simplify the simulations while preserving accuracy, hydrodynamic effects common to both the baseline ship (without WPS) and the Windship (with WPS), such as added resistance from ocean waves, windage, and hull fouling, are omitted, as they do not vary between the studied cases. Note that route optimization and unsteady effects are not considered in WindWise, ensuring identical wave conditions for both cases. Additionally, variations with negligible impact, such as sinkage, pitch, and heel-induced resistance (Gunnarsson and Egilsson, 2024), are omitted. Consequently, the computed overall savings and business case indicators remain the same.

The hydrodynamic side force Y_H and the induced associated resistance X_{Yi} as functions of leeway angle for Windships can be computed using simplified mathematical models. These models are often based on empirical methods from maneuvering research (Inoue et al., 1981), on wing theory for small aspect ratio wings (Tillig and Ringsberg, 2020), or the theory for ships without long keels (Schenzle, 1985), all of which are widely adopted in the literature. In WindWise, we use the approach proposed by Schenzle (1985) for sailing commercial ships without long fin keels. This approach was selected following a validation campaign in which we compared the various methods against the limited towing tank data available for commercial ships in oblique flow conditions. Fig. 3 shows the predictions of the non-dimensional hydrodynamic side force coefficient for the KVLCC2 tanker, as a function of leeway angle, for all three different approaches. These predictions are compared with the KVLCC2 towing tank test data presented in Kume et al. (2006).

As shown in Fig. 3, the Schenzle method provides the best match with the KVLCC2 towing tank results and is therefore the method employed in WindWise. This approach represents a generic model suitable for conventional commercial ship hulls, making

it particularly effective for retrofit simulations. However, it is important to note that this observation does not apply universally to all ship types. For example, Tillig and Ringsberg (2020) demonstrates that small aspect ratio wing theory yields better results for modern hull designs, such as the Ecoliner, which are specifically optimized for fully wind-powered operation. In contrast, the maneuvering derivatives outlined in Inoue et al. (1981) offer more accurate predictions for older ship designs. The discrepancies observed in the predictions between methods, as shown in Fig. 3 for the same ship hull, with average discrepancies exceeding 200% between the two extreme methods, lead to significant variations in the predicted performance of Windships and their overall business feasibility, depending on the approach applied. These inconsistencies emphasize the need for new generic yet accurate methods capable of rapidly assessing the performance of Windships across a diverse range of hull types. New preliminary studies, such as those presented in Reche-Vilanova et al. (2024b) and Van der Kolk and Freeman (2020), highlight this necessity and propose new methods, though these have not yet been widely validated. While acknowledging the limitations of the adopted approach (Schenzle, 1985), we deem it sufficiently accurate for integration into the hydrodynamic model. Furthermore, due to the modularity of WindWise, alternative methods or specific hull data—when available—can be employed for different ship hull types.

Schenzle (1985) separates the total hydrodynamic side force into two components: a linear cross-force term Y_{H1}, concentrated near the ship's bow and representing the deflected flow over the forward part of the hull due to the leeway angle, and a nonlinear cross-force term Y_{H2}, which arises from an end-plate effect caused by the "tip vortex" separating from the bottom or keel at an angle proportional to the leeway. For small leeway angles, Y_{H1} dominates the total side force, while for higher leeway angles ($\beta > 5deg$), Y_{H2} becomes increasingly significant. The total hydrodynamic side force Y_H is thus expressed as,

$$Y_H = Y_{H1} + Y_{H2} = \rho_w V^2 (k_1 T^2 \beta + k_2 T L_{WL}|\beta|\beta),$$ (6)

where L_{WL} is the length of the waterline, β is the leeway angle, and k_1 and k_2 are constant hydrodynamic factors. These factors are derived from oblique towing model tests and depend on parameters such as hull shape, heel angle, and propeller and rudder influence in the slipstream. Schenzle (1985) suggests indicative ranges for these constants in the absence of specific test results: k_1 is typically between 0.6 and 2, while k_2 ranges from 0.2 to 1.

The non-dimensional hull side force coefficient C_{YH} is calculated following,

$$C_{YH} = \frac{Y_H}{0.5\rho_w V^2 L_{WL}T} = 2k_1 \frac{T}{L_{WL}}\beta + 2k_2|\beta|\beta.$$ (7)

The corresponding induced drag due to the hull side force generation X_{Yi} is,

$$X_{Yi} = 2Y_H \tan\frac{\beta}{2}.$$ (8)

Thus, total hydrodynamic hull resistance X_H is defined as,

$$X_H = X_{CW} + X_{Yi}.$$ (9)

The longitudinal center of effort l_H of the hull side force generated as a function of the leeway angle is predicted using the equations proposed in Schenzle (1985) following,

$$l_H = \frac{l_{H1}Y_{H1} + l_{H2}Y_{H2}}{Y_{H1} + Y_{H2}},$$ (10)

where l_{H1} is assumed to be at the ship's bow and l_{H2}, at midship. This equation captures the trend of the center of effort shifting aft as the leeway angle increases, providing a realistic position trend under varying sailing conditions. The vertical center of effort v_H is assumed to be at half of the hull draft.

The added resistance due to heel, as well as the heel and drift coupling effects, are neglected in WindWise. The former is considered negligible, as indicated in Gunnarsson and Egilsson (2024), while the latter affects the side force prediction and alters the longitudinal center of effort, as discussed in Reche-Vilanova et al. (2024b). However, for small heel angles, the impact is assumed to be minimal.

The hydrodynamic heel moment, caused by the hull, rudder, and appendages, is calculated based on the side forces they produce under given weather conditions and a fixed center of effort at the midspan of each unit, as shown in Eq. (3).

On the other hand, the hydrostatic righting moment M_H is calculated from basic ship theory equations and approximations according to Rawson and Tupper (2001) following,

$$M_H = GM \Delta \sin \phi,$$ (11)

where GM is the transverse metacentric height, Δ is the ship displacement, and ϕ is the heel angle. The pitch moment and the buoyant force are not computed as they are not of interest in our 4 DoF calculations.

3.1.2. Rudder model
The rudder model calculates the lift L_R and drag D_R forces acting on the rudder using the methods outlined by Bertram (2012),

$$L_R = C_{LR}\frac{\rho_w}{2}V^2 A_R,$$ (12)

$$D_R = C_{DR}\frac{\rho_w}{2}V^2 A_R,$$ (13)

where A_R is the total area of the rudder, and C_{LR} and C_{DR} are the non-dimensional lift and drag force of the rudder, respectively, calculated following,

$$C_{LR} = 2\pi \frac{AR_R(AR_R + 0.7)}{(AR_R + 1.7)^2} \sin\beta + \sin\beta |\sin\beta| \cos\beta, \tag{14}$$

$$C_{DR} = 2.5 \frac{0.075}{(\log R - 2)^2} + \frac{C_{LR}^2}{\pi AR_R} + |\sin\delta|^3, \tag{15}$$

where AR_R is the aspect ratio of the rudder and $R = V c_R / \nu$ is the Reynolds number with c_R the rudder chord distance and ν the kinematic viscosity of the water. The longitudinal coordinate of the center of effort l_R for these forces is assumed to be located at 25% of the rudder's chord length. The vertical center of effort v_R is assumed to be at half of the total rudder height. The interaction effects between the hull and the rudder are not accounted in this calculation.

3.1.3. Appendages model

Hull appendages are designed to efficiently generate additional hydrodynamic side forces. If hull appendages are present in the windship, WindWise predicts their performance in terms of the lift L_A and drag D_A force generated following the methods presented in Hooft (1994) and Houghton and Carpenter (2003):

$$L_A = C_{LA} \frac{\rho_w}{2} V^2 A_A, \tag{16}$$

$$D_A = C_{DA} \frac{\rho_w}{2} V^2 A_A, \tag{17}$$

where A_A is the total area of the appendage, and C_{LA} and C_{DA} are the non-dimensional lift and drag force coefficients of the appendage, respectively, calculated following,

$$C_{LA} = \frac{2\pi}{1 + 2/AR_E} \sin\beta, \tag{18}$$

$$C_{DA} = C_{D0A} + \frac{C_{LA}^2}{\pi AR_E}, \tag{19}$$

where $C_{D0A} \approx 0.005 - 0.01$, and AR_E is the effective aspect ratio of the appendage. The longitudinal center of effort of the appendage model is assumed to be at 25% of the appendage chord. The interaction effects between the hull and the appendage are not considered.

3.2. Aero Model

The *Aero Model* calculates forces and moments for a wide range of Wind Propulsion System (WPS) configurations, considering variations in unit number, size, and deck arrangement, while maintaining a constant aspect ratio and a longitudinal arrangement as depicted in Fig. 2. The selected aspect ratio reflects current installations for each WPS class, ensuring realistic responses. Although currently restricted to longitudinal setups due to optimization constraints, the model is extendable to include side-by-side and zig-zag arrangements. The model also accounts for the aerodynamic interactions between WPS units and between the units and the ship hull. Interaction effects between WPS units and the superstructure are neglected. However, thanks to WindWise's modularity, if relevant data becomes available, these effects can be easily incorporated into the simulations. All aerodynamic force and moment computations are performed under typical Windship operating conditions, characterized by varying wind parameters (speed and direction), heel angles, and independent WPS unit trim settings.

A unique feature of the WindWise *Aero Model* is its ability to rapidly predict forces and moments across a wide range of independent sail trims for various WPS classes and configurations, each exhibiting distinct aerodynamic performance due to the unique interactions between units and the hull. This functionality is critical for optimizing fuel and emissions savings in Windships, as maximum thrust does not always correspond to maximum savings, as demonstrated in Reche-Vilanova et al. (2023).

The WindWise *Aero Model* provides two distinct approaches, depending on the WPS class being analyzed, to compute the relevant forces and moments. For passive systems, such as DynaRigs and Rigid Sails, which generate positive thrust without requiring continuous external energy, a machine-learning-based surrogate model is employed. This surrogate is developed from an extensive dataset of 3D computational fluid dynamics (CFD) simulations. On the other hand, for active systems, such as Rotor Sails, an analytical approach is utilized. This choice is driven by the particularly high computational cost and time required for CFD simulations of active systems and the limitations of the applied CFD solver in capturing the aerodynamics of these systems effectively. Each approach has distinct limitations and has been validated, as detailed in subsequent subsections.

All forces and moments are predicted/calculated at the WPS center of effort. The apparent wind speed is adjusted to the center of effort using the wind profile defined in Eq. (20).

To represent the atmospheric boundary layer, a power law relationship with an exponent of 0.11 is applied, which is a widely used approximation for open-ocean conditions (Hsu et al., 1994). The apparent wind speed is adjusted to the center of effort following,

$$V_{A_{Z_{CoE}}} = V_{A_{10}} \left(\frac{v_W}{10}\right)^{0.11}, \tag{20}$$

where V_A is the apparent wind speed and v_W is the vertical center of effort of the WPS.

3.2.1. Machine-learning surrogate for passive systems

WindWise employs machine-learning-based predictive surrogates to calculate the aerodynamic forces and moments for various Passive WPS configurations. The methodology, detailed in Reche-Vilanova et al. (2025), introduces a novel approach combining Computational Fluid Dynamics (CFD), independent sail trim optimization, and Machine Learning (ML) to develop surrogate models (Gaussian Process Regression and Feedforward Neural Networks) that predict aerodynamic responses with CFD-equivalent accuracy while significantly reducing computational cost.

The surrogate models are trained using an extensive 3D CFD aerodynamic database encompassing multiple WPS configurations, all optimized for maximum thrust via independent sail trimming. The inputs to the surrogate models include wind conditions, the number of units, mast spacing, and the independent trim of each unit. The models then predict the non-dimensional force coefficients C_{XW} and C_{YW}, along with the longitudinal and vertical centers of effort.

The database is validated against wind tunnel data to ensure reliability. The surrogates capture aerodynamic interactions between WPS units and between the units and the hull in a DynaRig case study, accounting for variations across a range of configurations and conditions. These models demonstrate high accuracy, with errors below 1%, enabling rapid design optimizations tailored to specific routes and wind conditions.

While the surrogates in this study focus on aerodynamic data for a single WPS class—the DynaRig—the models are designed to be applicable and expandable to other similar WPS classes, such as Rigid Sails and single-element inflatable systems.

Fig. 4(a) illustrates the percentage change in the maximum thrust coefficient for two passive wind propulsion systems in a longitudinal arrangement (one behind the other) compared to a single isolated unit generated by WindWise surrogates. Results are presented for different mast distance ratios, M_D (see Fig. 2 for reference), and correspond to the maximum thrust coefficient achieved when each unit is independently trimmed. Note that Fig. 4(a) does not represent fuel savings but rather a comparative analysis of the aerodynamic performance change due to interactions between units and mast spacing.

Fig. 4(a) highlights the critical role of modeling aerodynamic interactions between passive WPS to achieve realistic Windship performance predictions, particularly under close-hauled conditions. For a 2-unit configuration, a significant reduction in the maximum thrust coefficient, compared to a single isolated unit, is observed for apparent wind angles below 45 °, with the effect becoming more pronounced as the units are brought closer together. Conversely, a positive interaction is evident for the closely spaced configuration ($M_D = 1.1$) between 45 ° and 100 °. From 100 ° to 150 °, performance across all configurations aligns closely with that of an isolated unit, with wind shadowing effects causing reductions in thrust under near-downwind conditions. This shadowing effect becomes more pronounced for closely spaced DynaRigs. For 3-unit configurations, the magnitude of both positive and negative interaction effects is amplified.

The mass and corresponding weight of the DynaRig and other passive systems are estimated as a function of total sail area using data from manufacturers and open-source articles, such as Laursen et al. (2023). Passive systems in WindWise allow for user-defined reefing, which adjusts sail area, center of effort, center of gravity, and apparent wind speed range. This capability provides a significant advantage for reefable WPS classes, enabling sustained savings even under strong wind conditions. In contrast, non-reefable WPS classes must be taken down upon reaching maximum operating wind conditions, generating drag and increasing resistance instead of providing thrust.

3.2.2. Analytical approach for Rotor Sails

For a single Rotor Sail configuration, its corresponding aerodynamic forces and moments are generated as follows. Based on user-provided input, the tool defines a range of operating points between a non-rotating Rotor Sail and the maximum RPM specified by the manufacturer. For each operating point, the corresponding velocity ratio V_R, the key trimming variable for Rotor Sails, is calculated for various wind speeds:

$$V_R = \frac{\omega R_r}{V_A} = \frac{N \frac{2\pi}{60} R_r}{V_A}, \tag{21}$$

where $\omega = N 2\pi/60$ is the angular velocity and R_r is the Rotor Sail radius. For each velocity ratio, their corresponding lift C_L and drag C_D coefficients are extracted from the WindWise Rotor Sail database. This database is based on the Ackeret wind tunnel tests Prandtl and Betz (1932), which measured lift and drag coefficients as functions of velocity ratio for two aspect ratios, eight velocity ratios, and four end-plate sizes. Using these coefficients, the thrust and side force, along with the corresponding yaw and heel moments, are computed assuming the vertical center of effort v_W and center of gravity v_G of the Rotor Sail to be at half the total cylinder height. The longitudinal position of the Rotor Sail configuration, required for yaw moment computations, is assumed to be the geometric center of the arrangement. The mass and corresponding weight of the Rotor Sail is approximated as a function of the total sail area from data provided by the manufacturers (Norsepower, 2023).

Unlike the passive systems previously presented in this paper, Rotor Sails are active-rotating devices. Consequently, the power required to overcome frictional drag must be included for an accurate and realistic performance model. WindWise assumes that mechanical losses in the drive system and bearings are negligible compared to aerodynamic skin friction. The tangential viscous force on the spinning cylinder is estimated using flat plate boundary layer theory (Newman, 2018). The corresponding power requirement is then expressed as,

$$P_W = 0.5 \rho_a \pi A_W (\omega R_r)^3 C_{F_W}, \tag{22}$$

(a) *Passive systems.*   (b) *Rotor Sails.*
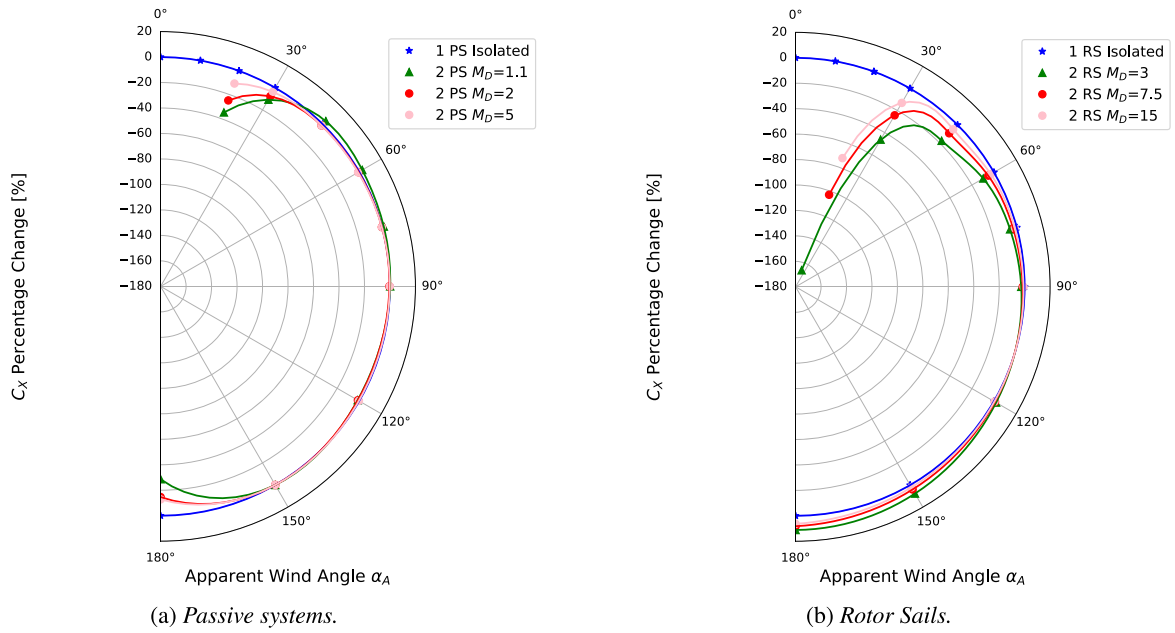
Fig. 4. Percentage of change in maximum thrust coefficient C_X due to aerodynamic interactions between a single isolated unit and three different configurations of two units and different mast spacing for both passive systems and Rotor Sails.

where πA_W is the surface area of the cylinder and C_{F_W} is the non-dimensional frictional coefficient approximated by Schlichting and Gersten (2016),

$$C_{F_W} = (2\log(R) - 0.65)^{-2.3} \; for \; R < 10^9. \tag{23}$$

The power consumption scales with the cube of the tangential velocity and is independent of the apparent wind speed. The accuracy of this approach was evaluated in Reche-Vilanova et al. (2021). If the Rotor Sails are equipped with end-plates, the additional surface area they introduce can be incorporated into the total spinning power calculation in Eq. (22).

When multiple Rotor Sails operate simultaneously, assuming the aerodynamic performance of a single unit multiplied by the total number of units does not provide sufficient accuracy. Aerodynamic interactions between devices lead to varying performance across wind conditions and WPS configurations. To model these interactions, the approach detailed in Garzón and Figueroa (2017), Tillig and Ringsberg (2020), Tillig (2020) is employed. This method divides the influence of Rotor Sails on the flow field over the ship's deck into two components: a potential part (circulation induced in the flow field) and a viscous part (wake and turbulence generated by flow separation and free vortices).

As outlined in Tillig and Ringsberg (2020), the potential flow influence generated by the bound vortex alters local wind speeds and directions across the ship, resulting in varying wind conditions for each WPS unit. This effect is modeled by analytically solving a simplified form of the Navier–Stokes equations for potential flow, under the assumption that the induced velocity from the WPS is zero at infinity and equal to the tangential speed V_t at the rotor surface. The tangential speed is caused by the circulation Γ responsible for generating the WPS lift, as described in Garzón and Figueroa (2017). Using this framework, the induced flow components in the x and y-directions can be computed as follows,

$$Vi_X(x, y) = \frac{V_t R_r}{\sqrt{x^2 + y^2}} \cos(\arctan(y/x)), \tag{24}$$

$$Vi_Y(x, y) = \frac{V_t R_r}{\sqrt{x^2 + y^2}} \sin(\arctan(y/x)). \tag{25}$$

As detailed in Garzón and Figueroa (2017), the solution for an array of rotors is derived by summing the induced flow from each individual rotor, accounting for the offsets of each rotor from the coordinate center (x, y). The tangential speed of a Rotor Sail can be calculated using the circulation, as described in Houghton and Carpenter (2003). An accurate relation between the lift coefficient and circulation Γ of a Rotor Sail is given in Swanson (1961), with approximated parameters as $k = 0.25$ and $\gamma = 210°$, based on good agreement with model test results for velocity ratios ranging from 1 to 4, as demonstrated in Swanson (1961).

Tip and root vortices are also generated at the top and base of the Rotor Sail. Their influences are modeled similarly to the bound vortex, with the primary distinction that these vortices are formed in the vertical plane (perpendicular to the inflow), as detailed in Tillig (2020). Consequently, the induced velocity components are first resolved into horizontal u_H and vertical parts before being
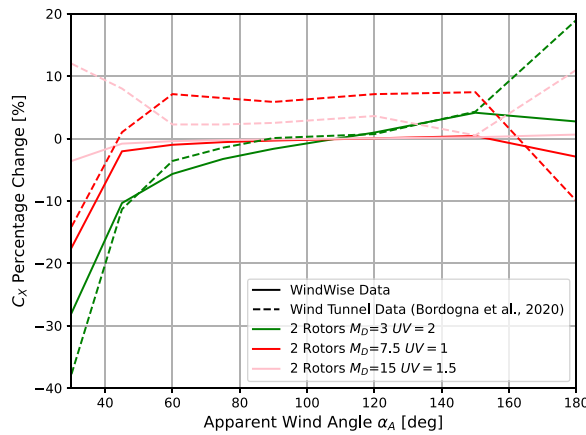
Fig. 5. Percentage of change of thrust coefficient C_X predicted by WindWise compared to wind tunnel data from Bordogna et al. (2020) for different Rotor Sails configurations and velocity ratios UV in longitudinal arrangement.

decomposed into $\ddot{u}_X$ and $\ddot{u}_Y$-components following,

$$Vi_H(x, y, h) = V_t \cos(\arctan(\frac{\sqrt{x^2 + y^2}}{\Delta h})), \tag{26}$$

$$Vi_X(x, y, h) = Vi_H \sin\alpha, \tag{27}$$

$$Vi_Y(x, y, h) = -Vi_H \cos\alpha. \tag{28}$$

Δh represents the distance between the tip or root and the Rotor Sail's vertical center of effort v_W. α is the apparent wind angle. In WindWise the circulation is assumed to be 80% of the bound vortex circulation, as indicated in Tillig (2020), Zuhal (2001). Assuming the ship's deck acts as a large endplate, the root vortex contributes 30% of the bound vortex circulation, while the tip vortex accounts for 50%. These vortices are assumed to align with the apparent wind angle, maintaining constant height, circulation, and radius as they extend downwind of the Rotor Sails.

Finally, viscous interaction effects caused by vortex shedding from the Rotor Sails are modeled. These are simplified by assuming a periodic fluctuation in the wind direction matching the local apparent wind angle and a 5% reduction in local wind speed within a corridor downwind of the units. The corridor width is equal to the Rotor Sail chord length and follows the potential streamlines. Note that the Rotor Sails Aero Model does not account for interactions between the units and the hull, unlike the surrogate model used for passive WPS.

The induced flow components in the x and y-directions, along with the reduction in local wind speed resulting from all the accounted for aerodynamic interactions, are added to the original wind conditions to calculate the updated local wind conditions for each unit. These induced flow components, along with their resulting aerodynamic forces and moments, vary depending on the relative positions of the units and their independent trim (velocity ratio). Consequently, generating a comprehensive aerodynamic response for multiple independent unit trims is essential. This response serves as input to the PPP to identify the optimal trim combination that maximizes overall performance.

Fig. 4(b) presents the percentage change in the overall maximum thrust coefficient for two Rotor Sails with an aspect ratio of 6, configured with different mast distance ratios M_D, compared to a single isolated Rotor Sail unit in a longitudinal arrangement. The results correspond to the resulting maximum thrust coefficient where each unit is trimmed independently to achieve maximum overall thrust.

This figure highlights the significance of modeling aerodynamic interaction effects between Rotor Sails, particularly under close-hauled conditions. A notable negative impact on the overall maximum thrust coefficient for a 2 unit configuration compared to a single isolated one is observed for all apparent wind angles smaller than 90 °, with the impact increasing as the rotors are more closely spaced. In contrast, a positive interaction occurs for all apparent wind angles greater than 90 °, with closely spaced rotors having the greatest positive effect. Fig. 4(b) also underscores the importance of route optimization for Rotor Sails, as their negative aerodynamic interaction in upwind conditions is substantial compared to passive systems. This is especially relevant for commercial ships which, due to their high sailing speeds, predominantly encounter apparent wind angles smaller than 90 ° (Fakiolas, 2023).

To validate the aerodynamic analytical approach for Rotor Sail performance presented in Tillig (2020), in conjunction with the WindWise aerodynamic database based on the work of Prandtl and Betz (1932), we compared the generated results with the wind tunnel test data for 2 Rotor Sails presented in Bordogna et al. (2020). The comparison is shown in Fig. 5. Unlike Fig. 4(b), it should be noted that the results in Fig. 5 correspond to equivalent Rotor Sails configurations at constant velocity ratios, fixed to match the wind tunnel data, across all apparent wind angles. Therefore, the rotors are not independently trimmed for maximum thrust in

Table 2
PPP Free Variables.

Condition	Free Variables	Valid Range
F_X	Engine Power	[0, MCR]
F_Y	Leeway Angle, β	[−10, 10] deg
M_X	Heel Angle, ϕ	[−12, 12] deg
M_Z	Rudder Angle, δ	[−25, 25] deg

this case. This plot serves purely for model validation. For this reason, the aerodynamic performance trends observed in Fig. 4(b), where each rotor was independently trimmed to maximize forward thrust, may differ from those in Fig. 5, where the settings were adjusted to match the experimental conditions of Bordogna et al. (2020) and validate the model.

Significant discrepancies can be observed between the two datasets. These variations may be attributed to the substantial uncertainties highlighted in the wind tunnel experiments reported by Bordogna et al. (2020) and differences in rotor geometry between the tested cases and those modeled in our predictions based on the WindWise aerodynamic dataset (Prandtl and Betz, 1932). However, the trends show good agreement with the wind tunnel test data. Notably, an increase in performance due to the interaction between closely spaced rotors downwind is observed for velocity ratios greater than 1.5. Conversely, a negative interaction is seen downwind for a low velocity ratio of 1 in the case of two rotors at a mast distance of 7.5, highlighting the importance of independently trimming the rotors to maximize performance across all apparent wind angles.

3.3. Engine and Propeller Model

WindWise uses an *Engine and Propeller Model* for assessing engine and propeller performance under hybrid operation with WPS. The model is presented in Reche-Vilanova et al. (2024a). For details, the interested reader is referred to the original paper. This generic and fast model combines empirical and analytical methods, requiring minimal input data. It predicts engine and propeller performance for simulated commercial ships equipped with WPS, accommodating Fixed Pitch Propellers (FPP) and Controllable Pitch Propellers (CPP) across two operational modes: constant ship speed; and constant shaft speed. The model captures changes in propeller and engine efficiency as a function of WPS net thrust, which is essential for realistic performance predictions under hybrid operation. By default, the propeller acts as a generator when surplus energy is available, contributing to the savings calculation outlined in Section 7. For pure wind-powered ships, the *Engine and Propeller Model* can be deactivated.

4. PPP model

The Performance Prediction Program (PPP) in WindWise, adapted from the NorthVPP (North Sails, 2019), models windship performance by balancing hydrodynamic, aerodynamic, and propulsive forces. It predicts theoretical sailing performance under varying wind conditions for a given ship configuration. For comparative analysis, WindWise runs the PPP model for both the *Baseline* (simulated ship without WPS) and the *Windship* (simulated ship with WPS) under identical sailing conditions, including speed and route. In *Baseline* simulations, only the *Hydro Model* and the *Engine and Propeller Model* are active. In *Windship* simulations, additional forces and moments from the WPS, as well as changes in engine load, propeller efficiency, and overall resistance due to aerodynamic and hydrodynamic effects, are included. Consequently, all models within the *Ship Model* are active.

4.1. Solution algorithm

The solution algorithm of the PPP model is formulated as a constrained NLopt SLSQP optimization problem (Kraft, 1988, 1994), expressed as,

$$\min f(x), \quad x \in \mathbb{R}, \quad x_{\min} \leq x \leq x_{\max}, \tag{29}$$

where f is the objective function and x is the vector of free variables. Table 2 lists the free variables and their respective valid ranges across the four degrees of freedom (DoF) considered in WindWise PPP. A valid solution satisfies equilibrium in forces and moments:

$$\sum F_X = \sum F_Y = \sum M_X = \sum M_Z = 0, \tag{30}$$

for a given set of environmental conditions. Sail trim optimization is a key aspect of the PPP model. The solver independently adjusts trim variables for each WPS unit to achieve the optimization objective—minimizing engine power in the PPP or maximizing sailing speed the VPP. Trim parameters are WPS-specific: mast rotation for DynaRigs, rotor RPM for Rotor Sails, and angle of attack for Rigid Sails. Each trim variable operates within defined upper and lower limits, ensuring optimal performance within physical and operational constraints.

5. Validation

This section presents and discusses the validation of the WindWise capability in predicting the performance of Windships across various Wind Propulsion System (WPS) classes. The validation is conducted through the comparison of predicted fuel savings and
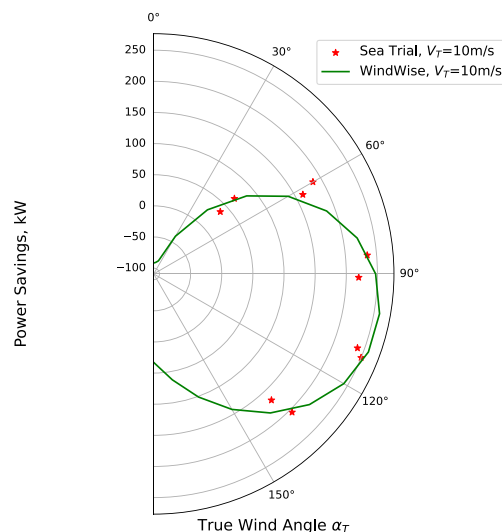
Fig. 6. Power savings from a single Rotor Sail on the M/S Annika Braren (Werner, 2022).

performance data for the few real-world vessels equipped with WPS technologies, ensuring the accuracy of WindWise's simulations in diverse operating conditions.

5.1. Annika Braren

The bulk carrier Annika Braren (IMO 9849148), fitted with an 18x3 meter Rotor Sail in April 2021, serves as the validation ship for this study. In September 2021, a speed trial was performed to evaluate the performance of the Rotor Sail under real operational conditions. The publicly available sea trial data, as documented in Werner (2022), is used here to compare the actual performance of the vessel with the WindWise prediction for the equivalent ship and Rotor Sail configuration under the exact same operating conditions.

The comparison of the predicted and measured power savings is shown in Fig. 6. WindWise's prediction aligns closely with the observed performance for a single Rotor Sail installed at the bow of the Annika Braren, despite the Rotor Sail Aero Model not accounting for WPS unit-hull interaction effects. This suggests that the simplified model effectively predicts the Rotor Sail's performance in this configuration. However, the lack of hull interaction modeling represents a limitation for configurations with multiple rotors or different placements, where such effects may be more significant.

The error in power required for calm water, as compared with the sea trial data from Werner (2022), is less than 1%, indicating that WindWise's hydro models accurately represent the vessel's propulsion in calm conditions. Regarding fuel savings, WindWise predicts an average fuel savings of 2.02% for this ship typical North Spain to Baltic Sea route. This prediction aligns well with the 2–4.5% range reported in Werner (2022)'s performance prediction program, further validating WindWise's accuracy when compared to other existing tools.

These results highlight the reliability of WindWise in simulating Windship performance specifically with Rotor Sails. However, it also validates the full ship model, including the hull, rudder, and engine and propeller model. The only model that could not be validated with sea trial data is the DynaRig aero model, however, since this model itself was validated in Reche-Vilanova et al. (2025) against wind tunnel data, it is assumed to also be validated.

6. Route and weather model

The *Route and Weather Model* in WindWise allows performance simulations using either a specific route or a global IMO route (MEPC, 2021). This simplified model does not optimize routes for maximizing WPS performance but supports WindWise's Cost–benefit and design optimization goals. A more detailed method may replace it in the future.

6.1. Specific route

For route-based simulations, users input departure and destination points, optionally specifying calling ports. The route model computes the shortest path while avoiding landmasses using the Haversine formula (Van Brummelen, 2017), dividing it into waypoints with a maximum spacing of 100 nautical miles (see Fig. 7). Weather conditions at each waypoint are derived from the ERA5 dataset (Hersbach et al., 2020) (2000–2022), using yearly-averaged data recalculated in ship-heading coordinates. If specific departure dates are required, the same *Specific Route* model can be applied without modification, provided the corresponding weather
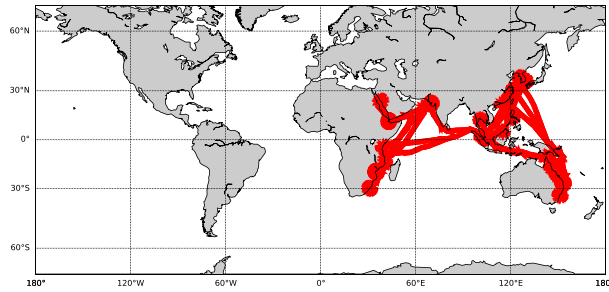
Fig. 7. Example of a commercial ship route simulated over one year using the Specific Route option in the WindWise *Route and Weather Model*.

data is available. Using these conditions at each waypoint, the model estimates ship performance based on the results from the *PPP Model*. This performance is then converted into fuel consumption and emissions for each waypoint. Total savings for the entire route are obtained by aggregating savings across all waypoints.

6.2. IMO Wind Statistics

As an alternative to a specific route, the IMO Wind Statistics model can be used to simulate fuel and emissions savings over the most common global shipping trade routes. For this, the global wind probability matrix provided by the International Maritime Organization (IMO) is employed (MEPC, 2021). The wind probability matrix used in this model is the same one approved for calculating the Energy Efficiency Design Index (EEDI), as discussed in Section 7.4.

7. Cost model

The *Cost Model* is organized into four primary categories: Capital Expenditures (CAPEX), Operational Expenditures (OPEX), business case indicators, and IMO ship carbon intensity indexes. This model evaluates the financial impact of Wind Propulsion System (WPS) installations and operations by calculating initial investment costs, ongoing operational savings, potential penalties, and overall financial viability across varying scenarios. Additionally, it assesses the ship's performance relative to IMO carbon intensity indices, offering insights to support informed decision-making regarding the integration of WPS technologies.

7.1. WPS CAPEX calculation

The WPS CAPEX module calculates the initial investment required for different WPS classes. The framework considers variables such as sail area, number of units, and tiltable system features, with installation costs modeled as a percentage of the CAPEX. Manufacturing costs are estimated based on component raw material expenses, labor rates, tooling costs, and gross margins. Economy of scale is applied by distinguishing between constant and variable costs, depending on the number of units and total sail area. These include:

- Constant costs: Engineering, administrative, and design costs.
- Variable costs based on WPS units: Trimming equipment, sensors, and anemometers.
- Variable costs based on sail area and units: Material, labor, and tooling costs.

Thus, the WPS CAPEX is modeled as,

$$\text{CAPEX} = (a \cdot A_W + b \cdot |A_W - A_r| + c) \cdot n + d \tag{31}$$

where A_W represents the sail area per unit, n is the number of units, and A_r is the reference sail area provided by the manufacturer, considered the standard or most cost-effective solution for each WPS class. Note that A_r is constant. The constants a, b, c, and d, with $b < a$, are derived from WindWise private WPS cost database, which incorporates both confidential manufacturer and open-source data sources (Laursen et al., 2023). While the structure of the equation remains consistent across all WPS classes, the values of a, b, c, and d differ by class, reflecting their respective pricing characteristics. The non-linear increase in material, labor, and tooling costs for units with sail areas deviating significantly from the reference A_r is currently approximated using a piecewise linear function through the term $b|A_W - A_r|$. This approach captures the global non-linearity of CAPEX with respect to the reference area but does not account for exponential cost growth in very large systems, due to limited CAPEX data across WPS classes, sizes, and units in the current WindWise database. As additional data becomes available, Eq. (31) could be refined with non-linear terms, enhancing representation of cost dynamics across different WPS classes and configurations.

For tiltable systems, an additional 20% is added to the total CAPEX to account for the increased complexity and weight of the system, unless otherwise specified. If installation costs are not available, WindWise assumes them to be 2% of the total CAPEX (Laursen et al., 2023).

7.2. OPEX calculation

Operational expenditures (OPEX) for both the baseline and Windship scenarios are systematically evaluated to quantify the gains and losses between the two cases. This analysis is critical for simulating the business case for each WPS installation.

The objective of this calculation is not to provide a comprehensive overview of the ship's OPEX, such as revenue from cargo or crew salaries. Instead, the focus is on the specific OPEX components that differ between the baseline and Windship scenarios. All other variables not explicitly addressed are assumed to remain constant across both cases.

WindWise includes the following OPEX components in its calculation:

- Fuel costs
- Carbon emissions costs
- WPS Maintenance costs
- Cargo space lost cost

As anticipated, fuel consumption and corresponding pollutant emissions will differ between scenarios. The total costs associated with these factors also vary based on fuel prices and emissions pricing scenarios.

The maintenance costs of the WPS installation are included as an additional expense unique to the Windship scenario. Similarly, the introduction of WPS systems on commercial ships may result in added weight and volume constraints. These can lead to increased hydrodynamic resistance at a given speed or a reduction in net tonnage due to stability and draft limitations. Furthermore, WPS components may occupy valuable volumetric cargo space, particularly if they encroach upon cargo holds or tanks. If these impacts are not mitigated, they reduce the ship's payload capacity, which must be reflected in the cost calculations.

The total OPEX saved between *Baseline* (B) and *Windship* (W) is calculated as follows,

$$OPEX_S = OPEX_B - OPEX_W \tag{32}$$

where $OPEX_B$ is defined as,

$$OPEX_B = F \cdot C_F + E \cdot C_C \tag{33}$$

where F is the fuel consumption, C_F is the fuel cost, E are the absolute emissions, and C_C carbon tax in terms of cost per tonne of pollutant emissions emitted. On the other hand, $OPEX_W$ is defined as,

$$OPEX_W = (F \cdot C_F + E \cdot C_C) - (C_M + C_{CL}) \tag{34}$$

where C_M are the maintenance costs-equivalent and C_{CL} are the cost of cargo lost for that specific route. C_M is computed following,

$$C_M = \frac{C_{M_t}}{D_y} \tag{35}$$

where C_{M_t} is the yearly maintenance costs which are divided by the total yearly days D_y at sea. Thus, we can model a daily maintenance cost-equivalent value for each route. The yearly maintenance costs, if unknown, are approximated as a 2% of the total CAPEX of the WPS installation (Laursen et al., 2023).

WindWise models the cost of cargo space lost due to WPS installation as follows. In cases where the ship is not fully loaded or operating under ballast, the additional weight of the WPS installation is first offset by reducing ballast and then by utilizing available cargo capacity. If further compensation is required, users can define whether this can be achieved by reducing fuel capacity, potentially leading to shorter ranges and more frequent refueling. Under these conditions, the WPS weight is considered negligible, resulting in no income loss or additional costs. Consequently, the WPS device can be installed without impacting the ship's payload capacity.

However, when the ship is fully loaded and unable to reduce ballast or fuel capacity, the cost of lost cargo space due to the additional weight and volume of the WPS must be accounted for. For deck-mounted WPS systems on ships such as tankers and bulk carriers, volume impact is typically negligible. However, this becomes significant for keel-mounted systems, which may encroach upon tank space, or for containerships, where deck space for containers is compromised. These volumetric limitations are user-defined in WindWise. If deemed negligible, only the cost of lost weight is considered. Otherwise, both weight and volume impacts are evaluated, with the limiting factor dictating the final calculation.

The cost of lost cargo space (C_{CL}) is calculated as follows, depending on the contract type:

1. *Voyage (Spot) Charter*: The freight rate is expressed in USD per ton of payload (S). For a single round trip,

$$C_{CL} = W_W \cdot S \tag{36}$$

   To estimate the annual cost, this value is multiplied by the number of round trips per year. Spot rates are highly variable and route-dependent, necessitating scenario-based analysis.

2. *Time Charter*: The freight rate is expressed in USD per deadweight ton per month (T_C). For a single month,

$$C_{CL} = W_W \cdot T_C \tag{37}$$

   To calculate the annual cost, this value is multiplied by the operating months per year. As with spot rates, time charter rates are subject to variation, requiring scenario-based evaluations.

WindWise allows users to specify the ship's loading conditions and determine whether adjustments to fuel or ballast capacity can mitigate the WPS weight impact, enabling more accurate cost estimations.

7.3. Business case indicators

WindWise evaluates the economic feasibility of WPS adoption by computing three key business case indicators: the payback period PBP, the net present value NPV, and the time required to achieve $NPV = 0$.

The payback period is defined as,

$$PBP = \frac{CAPEX}{OPEX_S} \tag{38}$$

This metric represents the time required for the savings in operational expenditures $OPEX_S$ thanks to the WPS installation to offset the capital expenditure $CAPEX$. However, the payback period does not account for the time value of money or the scale of the investment. Therefore, WindWise also computes the NPV which represents the net financial benefit or cost of an investment over its lifetime, expressed in present value terms. It is defined as,

$$NPV = \sum_{p=0}^{n} \frac{OPEX_S}{(1 + i)^p} - CAPEX \tag{39}$$

where i is the discount rate, p is the year, and n is the number of years. To determine the number of years required to achieve $NPV = 0$, Eq. (39) is solved iteratively to find the value of p that satisfies the condition $NPV = 0$.

WindWise computes these indicators under user-defined scenarios, incorporating variables such as fuel prices, emissions regulations, and operational parameters (e.g., days at sea, route-specific weather conditions). This enables a scenario-specific evaluation of the economic viability of WPS implementation for a given ship. For retrofitted ships, the vessel's remaining operational life must be specified, while for new builds, a maximum service life is defined.

7.4. IMO Indexes

WindWise calculates the Carbon Intensity Indicator (CII) as specified by the International Maritime Organization (IMO) to evaluate the carbon intensity of a ship's operations (IMO, 2022a,b,c). The CII is computed for both Baseline and Windship scenarios, allowing for a direct comparison of CII ratings in each condition. To address potential overestimation of the Baseline CII due to neglecting added resistance from ocean waves, an additional 30% fouling and sea margin is applied to fuel consumption in both scenarios (Carlton, 2018). However, the difference in CII ratings between the two scenarios is assumed unaffected by this adjustment.

For the Energy Efficiency Design Index (EEDI), only the Windship scenario is considered, as the focus is on calculating the power deduction achieved by the WPS installation. According to IMO guidelines (MEPC, 2021), the power reduction from wind-assisted propulsion is subtracted from the total required propulsion power in the EEDI calculation. This reduction results in a lower required propulsion power, contributing to improved energy efficiency for the commercial ship.

8. Optimizer

The WindWise Optimizer uses a Particle Swarm Optimization (PSO) (Bonyadi and Michalewicz, 2017) algorithm to identify the optimal Wind Propulsion System (WPS) configuration for a given vessel and simulated route. This optimization process, which is constrained by specific design and operational limits, can be formally expressed as shown in previous Eq. (29). It is important to note that WindWise focuses exclusively on optimizing the WPS installation, modifying only the WPS configuration to meet the selected optimization goal, while excluding changes to the ship hull or other factors that may affect overall performance, as illustrated in the WindWise diagram in Fig. 1.

The WPS configuration space may exhibit non-smooth and non-continuous characteristics. Gradient-based optimizers are prone to get stuck in local minima, especially in complex, non-linear search spaces. PSO is particularly well-suited for this application by overcoming these limitations by efficiently navigating such spaces and identifying global optima, even in the presence of local minima. This flexibility allows WindWise optimizer to adapt to a wide variety of WPS configurations, vessel characteristics, and route conditions.

WindWise optimizer objective is user-defined and can be one of the following:

1. Minimizing the payback period (PBP)
2. Maximize the net present value (NPV)
3. Maximizing fuel savings

The objective is achieved by adjusting the following key WPS configuration variables, with the valid ranges for each WPS class presented in Table 3,

1. Sail Area
2. Deck position
3. Number of units

Table 3
Optimization variables and valid ranges for each WPS class under investigation.

Parameter	Valid Range	
	DynaRigs	Rotor Sails
Sail Area	500–2000 m^2	50–400 m^2
Deck position	bow-aft	bow-aft
Number of units	1–3	1–5
Spacing between units	$1.1 \leq M_D \leq 5$	$3 \leq M_D \leq 15$

4 Spacing between units

The user can set how many of the previous configurations variables are required to be optimized, from a single one to all of them, as well as the valid ranges for each of the variable. If more variables are required, the total number of particles and iterations must be increased to achieve a converged solution. The algorithm evaluates the vessel's performance under these configurations and searches for the combination that yields the most favorable financial and environmental outcomes. As described in Section 4, the sail trim of each unit is adjusted independently to maximize the optimizer objective.

8.1. Optimizer constraints

The optimization process integrates several practical constraints to ensure that the proposed Wind Propulsion System (WPS) configurations are both realistic and feasible for real-world applications while meeting predefined emissions reduction targets. These constraints include:

1. *Minimum Savings Target*: The optimizer ensures all WPS configurations meet predefined emissions reduction targets. Configurations failing to do so are penalized and discarded, prioritizing solutions that achieve the required savings.
2. *Maximum Air Draft*: The air draft, defined as the vertical distance from the waterline to the WPS's highest point, must not exceed the vessel's limit to ensure safe navigation under bridges and into ports. This constraint is waived for retractable WPS systems.
3. *Feasible Deck Positions*: WPS installations must fit within the vessel's deck boundaries, respecting its maximum length. By default, placement is unrestricted, but user-defined positions can limit the optimizer to specific areas, ensuring practical feasibility.

These constraints ensure that the proposed WPS configurations are technically feasible, operationally viable, and aligned with the desired optimization objectives—whether that is to maximize fuel savings, enhance operational efficiency, or improve the overall business case viability for WPS installation.

8.2. Assumptions and limitations

Due to WindWise modeling limitations, the optimizer assumes all units within a configuration belong to the same WPS class, with constant sail area, aspect ratio, uniform spacing, and a longitudinal deck configuration Fig. 2. These assumptions simplify the optimization process and reflect common WPS designs but may not fully capture all real-world configurations.

The DynaRig WPS class is limited to a maximum of 3 units, while Rotor Sails can have up to 5 units. This constraint is not expected to significantly impact results, as DynaRigs, being larger systems, typically achieve similar fuel savings with fewer units. WindWise is designed to predict realistic configurations for each WPS class while maintaining computational efficiency.

For Rotor Sails optimization, maximum rotational speeds (rpm) are limited based on sail size, adjusted according to manufacturer specifications (Norsepower, 2023). However, the model does not account for noise and vibrations from high-speed rotation of large Rotor Sails.

9. Results: Case study

WindWise was applied to a case study of a single-screw, diesel-driven, 50,000 DWT oil tanker with key specifications listed in Table 4. The vessel represents a real 5-year-old ship with a conventional hull, making it a suitable candidate for retrofit WPS design optimization. The simulated service speed is 12 knots, powered by a four-bladed fixed-pitch propeller (FPP) and a main engine output of 7585 kW at MCR.

For this particular case study, the WindWise optimizer was set to identify the most cost-effective configuration for both DynaRigs and Rotor Sails by minimizing the payback period (optimizer objective) while ensuring compliance with the minimum emissions reduction targets set by the 2023 IMO GHG Strategy (MEPC, 2023) (optimizer constraint). Although minimization of the payback period was the main objective, the net present value (NPV) was also evaluated for a more comprehensive investment analysis.

Two main retrofitting scenarios were analyzed:

1. *Ideal*: Assumes no cargo space loss and no air draft limitations, applying the cost assumptions from Section 7.2.

**Table 4**

Simulated oil tanker main particulars.

Parameter	Dimension
Length Over All (L_{OA})	183 m
Beam (B)	32 m
Draft (T)	13.30 m
Ship Speed (V)	12 kn
MCR	7585 kW

Table 5

Route and fuel and market-based measures (MBM) scenarios.

Route Scenario	Departure	Arrival
1 - IMO Wind Statistics	–	–
2 - Atlantic Route	Houston (USA)	Rotterdam (NL)
Fuel & MBM Scenario	Fuel Price	MBM Price
1 - Green Marine Fuel	2000 \$/ton	0 \$/ton
2 - Carbon Tax	700 \$/ton	150 \$/ton
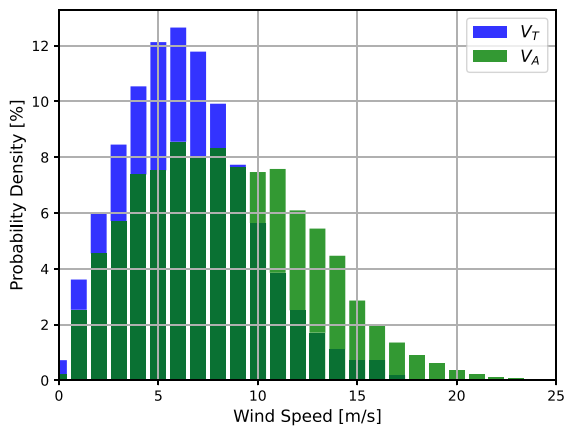
(a) *Wind Speed.*
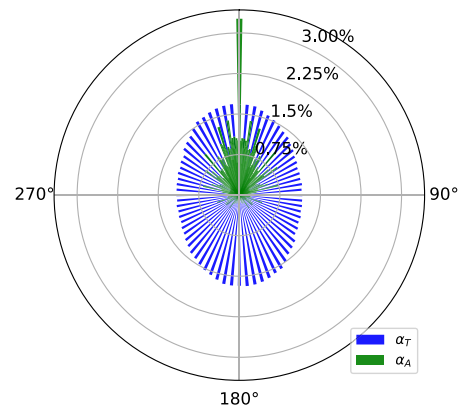
(b) *Wind Angle.*

Fig. 8. IMO Route Wind Statistics and resulting apparent wind speed and angle probability for the simulated ship speed.

2. *Realistic*: Considers the monetary impact of cargo space loss Section 7.2 and imposes a maximum air draft. WPS exceeding the air draft must adopt tilting systems, adding weight and cost Section 7.1.

The *Ideal* retrofitting scenario was analyzed across two route scenarios and two fuel and market-based price scenarios (Table 5). In contrast, the *Realistic* retrofitting scenario was only simulated for the Atlantic Route under the Carbon Tax scenario.

The first route uses IMO Wind Statistics, representing global trade averages. Apparent wind conditions derived from simulated sailing speed and true wind speed and angles are shown in Fig. 8. This route represents a less favorable wind conditions scenario. The second route, from Houston to Rotterdam, is representative of crude oil tanker operations and features higher wind speeds and more favorable wind angles Figs. 9(a) and 9(b), offering better wind propulsion potential.

For the fuel and market-based (MBM) scenarios, scenario 1 assumes a future case with 100% green marine fuel and no carbon tax. Scenario 2 represents a business-as-usual scenario with conventional fuel and carbon pricing reflective of potential EU ETS projections.

The assumptions, limitations, and detailed results of these scenarios are discussed in the following subsections.

9.1. Use case assumptions and limitations

The following assumptions and limitations apply to the WPS installation optimization in this tanker retrofit use case:

1. Wind Propulsion Systems:

   • DynaRigs are assumed to be reefable when maximum operating wind conditions are reached. Reefing begins with the top sails, thereby lowering both the vertical center of effort and the center of gravity.
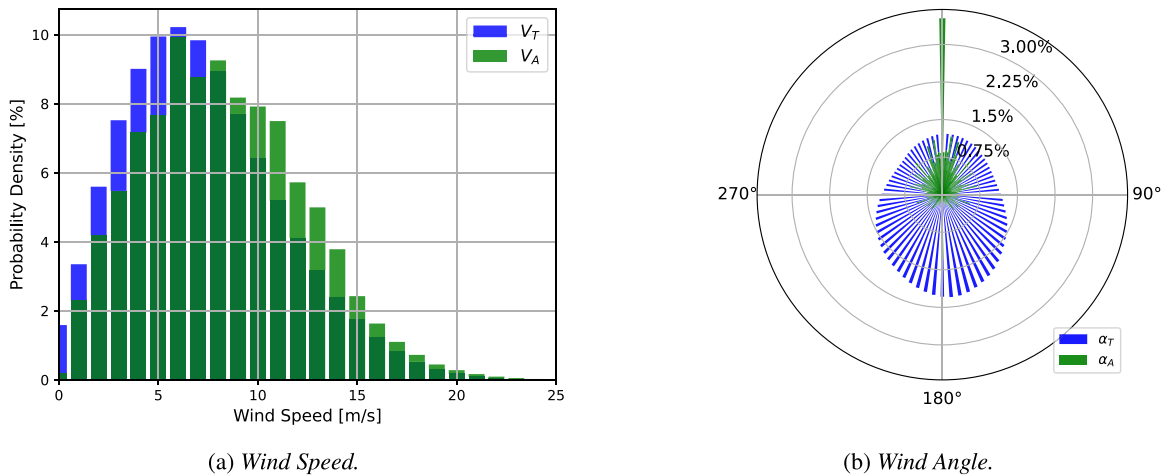
(a) *Wind Speed.*

(b) *Wind Angle.*

Fig. 9. Houston-Rotterdam Atlantic Route Wind Statistics and resulting apparent wind speed and angle probability for the simulated ship speed.

- Rotor Sails are designed to operate up to a maximum wind speed of 30 m/s, as specified by the manufacturer (Norsepower, 2023). Beyond this threshold, they are set to a non-spinning mode.
- The aspect ratio of the DynaRigs is fixed at 2.4, while that of the Rotor Sails is fixed at 6.
- Based on manufacturer specifications, the weight of a 1000 m^2 DynaRig is set to 40 tonnes, while the weight of a 175 m^2 Rotor Sail is 80 tonnes (Norsepower, 2023).
- Typical sail areas for each WPS class available in the market are used in this study, along with an upper and lower range to explore potential expansion possibilities.

2. Route and Weather:

- No route optimization is applied Section 6.
- Weather predictions are based on historical data.
- The vessel operates on the studied route for 280 days per year.

3. Costs:

- A 3% interest rate is used for the NPV calculation.
- The ship's total life expectancy is assumed to be 25 years.
- The remaining years considered for the NPV calculation are 20 years.
- The average spot rate is 25$ per metric ton of payload for the ship's typical cargo and routes (Lagouvardou et al., 2022).
- EEDI and CII ratings are not evaluated in this study, as the ship is new and already features favorable carbon intensity metrics.

4. Optimization:

- Only longitudinal WPS deck arrangements are considered as depicted in Fig. 2.
- The maximum number of DynaRig units is set to 3, while Rotor Sails can have up to 5 units.
- Full deck availability for WPS installation is assumed, disregarding constraints like interference with other onboard structures.
- Visibility requirements for the ship's operations are not accounted for.

The results presented are valid within these optimization assumptions and general WindWise solver assumptions and limitations previously presented. Changes in these scenarios may lead to different outcomes and optimal configurations. This study does not evaluate the CII rating impact of WPS, as the use case involves a relatively new ship with the highest existing CII rating. In its current state, WPS does not enhance the baseline rating. However, under future stricter CII rating standards, WPSs could provide significant benefits. WPS serve as both a compliance tool and a business case enhancer, potentially improving ratings, reducing operational costs, supporting compliance with mechanisms like FuelEU, and enabling participation in pooling mechanisms, particularly for less energy-efficient ships.

Future studies will address the assumptions and limitations outlined here, expanding the scope to include additional variables and scenarios. The primary aim of this work is to demonstrate the advantages of optimization of WPS configurations, with broader considerations left for future exploration.
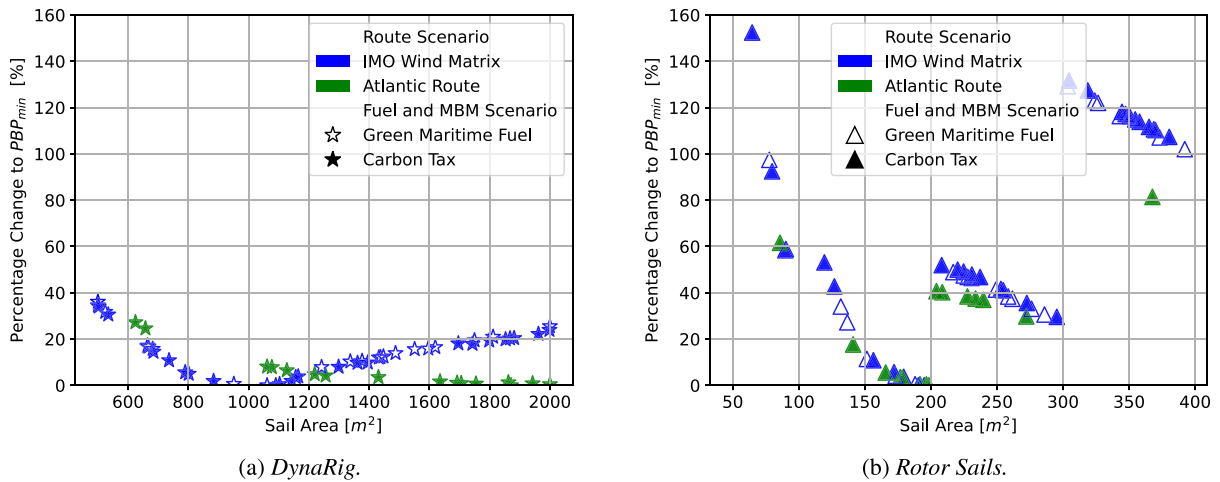
Fig. 10. Percentage of change to minimum Payback Period PBP_{min} as function of sail area per unit for DynaRigs and Rotor Sails for both route scenarios and both fuel and MBM scenarios.

9.2. Optimization scenario: Ideal

In this scenario, the result evaluation is divided into two stages: a parametric study and a full optimization. In the parametric study, the payback period is analyzed by adjusting one of the four WPS configuration variables (sail area, deck position, number of units, and spacing between units) while keeping the other three fixed. This process is repeated independently for each configuration variable, WPS class, and route/price scenario. The goal is to understand the performance trends of each WPS class, isolate the impact of each configuration variable, identify their strengths and weaknesses, and emphasize the importance of optimizing WPS installations for cost-effectiveness.

In the full optimization, the payback period is optimized by adjusting all four WPS configuration variables simultaneously for each WPS class and route scenario. This stage aims to identify the best WPS installation across all variables, minimizing the payback period for each WPS class and route.

9.2.1. Parametric study

Fig. 10 illustrates the percentage change in the predicted payback period relative to the minimum value found for each WPS class, as a function of typical sail area per unit, with a single WPS unit placed at midship. The results emphasize the importance of optimized installations to maximize cost-effectiveness. DynaRigs show deviations in payback period of up to 40% from the optimal value, while rotor sails exhibit deviations exceeding 150%. These findings underscore the crucial role of optimization in unlocking the full potential of WPS installations and maximizing investment returns. Additionally, Fig. 10 highlights the performance differences between the two WPS classes.

DynaRigs Fig. 10(a) show a smoother trend across both route and fuel/market-based scenarios. For the IMO Wind Matrix, where most conditions are close-hauled, the trend is concave, with the most cost-effective sail area around 1000 m^2. Smaller rigs are less effective due to their lower aerodynamic center of effort, limiting access to higher wind speeds in the atmospheric boundary layer, and the lack of proportional cost reductions from fixed unit costs. Larger rigs, on the other hand, incur penalties from higher manufacturing costs and added weight. On the Atlantic route, where wind conditions are more favorable, fuel savings increase Fig. 11(a), making larger sail areas more cost-effective, as reflected in the linear decreasing trend.

On the other hand, Rotor Sails Fig. 10(b) exhibit a multi-step trend across both route and fuel/market-based scenarios, driven by their performance dependency on size and maximum rpm limits, as discussed in Section 3.2.2. Each step corresponds to a fixed maximum rpm limit, with larger rotor sail areas becoming more cost-effective under these fixed rpm limits. This trend aligns with industry movements towards larger rotor sails, where increasing the radius while maintaining aspect ratio enhances aerodynamic performance, reduces spinning power consumption, and broadens the operational wind speed range. It is important to note that rotor sail areas exceeding the current market maximum of 175 m^2 are modeled using extrapolated trends beyond available manufacturer data (Norsepower, 2023). For both routes, the optimal Rotor Sail configuration is approximately 200 m^2 of sail area. Larger areas incur higher costs due to engineering complexities and added weight, as detailed in Section 7. However, on the Atlantic route, favorable wind conditions help mitigate this penalty by increasing fuel savings Fig. 11(b).

Figs. 11(a) and 11(b) highlight the impact of route and weather conditions on fuel savings as a function of sail area. As expected, both WPS classes show steeper fuel savings on the Atlantic route due to more favorable wind conditions. However, Rotor Sails do not exhibit a consistent increase in fuel savings with increasing sail area across all scenarios. Instead, they peak at 300 m^2 on the IMO Wind Matrix route Fig. 11(b), where close-hauled conditions increase side forces and hydrodynamic resistance, causing savings to decline beyond that point. In contrast, on the Atlantic route, where side-wind conditions mitigate these penalties, Rotor
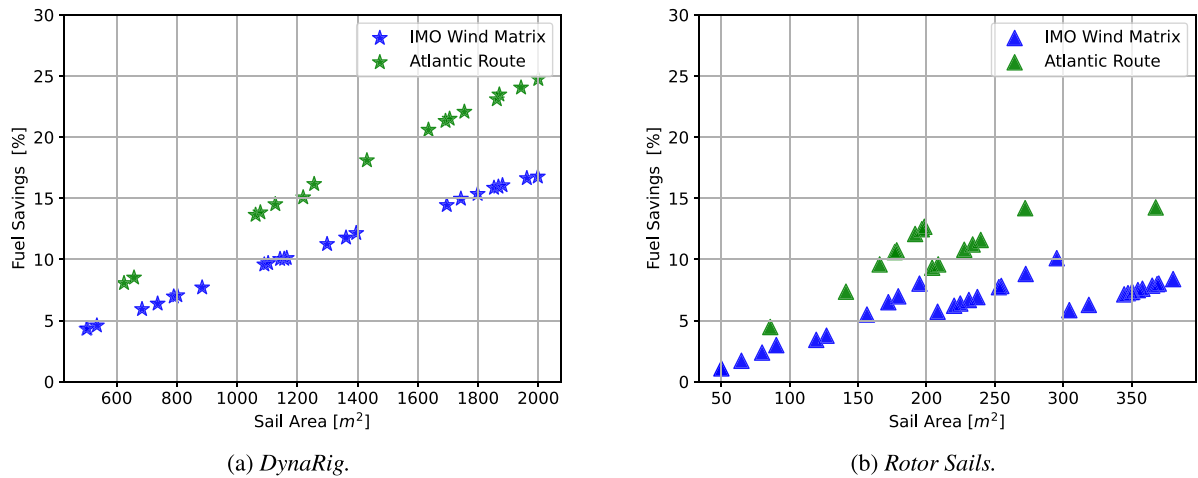
Fig. 11. Fuel savings as function of sail area per unit for DynaRigs and Rotor Sails for both route scenarios.
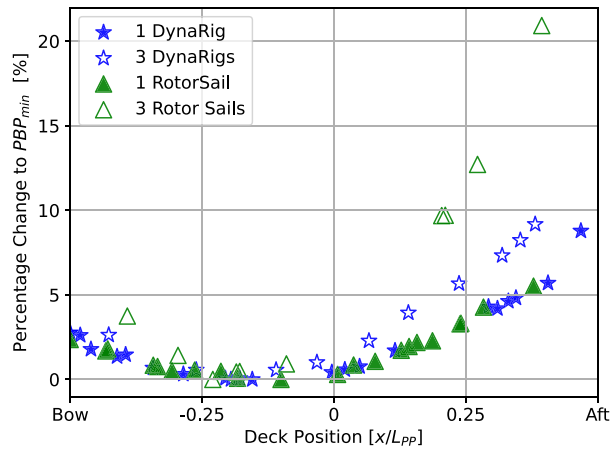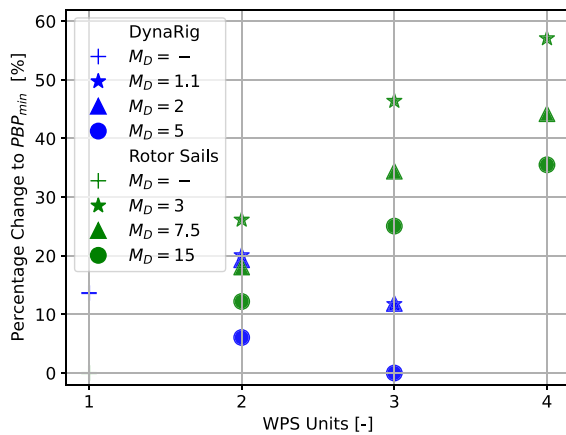

Fig. 12. Percentage of change to minimum Payback Period PBP_{min} as function of deck position for DynaRigs and Rotor Sails. Note that the deck position is defined as the location of the geometric center of effort of the WPS configuration under study.

Sails maintain higher savings at larger sail areas. Additionally, Rotor Sails are the most compact WPS option, achieving the highest fuel savings per square meter of sail area, making them ideal for installations with strict air draft constraints, as noted in previous studies such as Reche-Vilanova et al. (2021).
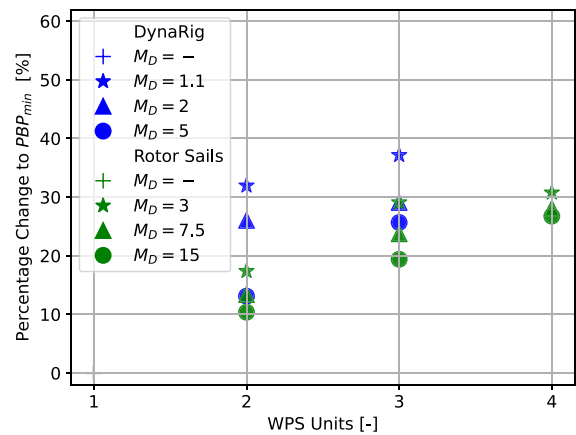
The different fuel and market-based scenarios presented in Fig. 10 lead to reduced payback periods. However, as shown, the trends in sail area that minimize the payback period remain consistent across the various cost scenarios, making their impact on the optimal WPS configuration negligible. Therefore, all subsequent analyses will focus on the more realistic Fuel Scenario 2 (Carbon Tax Scenario) for simplicity.

Fig. 12 illustrates the impact of deck placement on payback period for each WPS class, focusing on the IMO Wind Statistics route. Both WPS types perform best when placed near the hydrodynamic center of lateral resistance, approximately midway between the midship and bow. Positioning farther from this point increases yaw moment, requiring more rudder deflection, hence increasing the rudder's induced drag, and thus reducing savings potential, as detailed in Reche-Vilanova et al. (2023). The IMO Wind Statistics route, with higher close-hauled conditions and increased side forces, amplifies the effect of deck placement, whereas the Atlantic route, with less side force due to more favorable side-wind conditions, shows less sensitivity. Rotor Sails, due to their lower lift-to-drag ratio and higher side forces compared to DynaRigs for the same amount of thrust delivered, are more sensitive to deck placement. For the larger installations studied here (e.g., 3 units), Rotor Sails exhibit up to a 20% increase in payback period when placed suboptimally, while DynaRigs show a maximum change of less than 10%. As the number of units increases, the sensitivity to deck placement becomes more pronounced, particularly for high side-force generators like Rotor Sails, further emphasizing the importance of optimal deck placement for maximizing savings.

Fig. 13 shows the percentage change in the predicted payback period relative to the minimum value, based on the optimal sail area and deck placement for each WPS class, as a function of mast spacing (M_D) and number of units for each route scenario.

(a) *Route 1: IMO Wind Statistics.*   (b) *Route 2: North Atlantic.*

Fig. 13. Percentage of change to minimum Payback Period PBP_{min} as function of units and relative mast spacing for DynaRigs and Rotor Sails for both route scenarios.

Both WPS classes experience reduced payback periods with increased mast spacing, highlighting the importance of distance in minimizing negative interaction effects. However, for DynaRigs on the IMO Wind Matrix route, where close-hauled conditions prevail, a closer spacing ratio (D_M=1.1) is as cost-effective as a wider spacing (D_M=2). This is due to the performance balance between the favorable aerodynamic interactions at D_M=1.1 and the reduction in upwind penalties for D_M=2 (see Fig. 4(a)). In contrast, D_M=5 configuration, while lacking positive interactions, compensates with significantly lower upwind penalties, leading to better overall performance. On the Atlantic route, where wind conditions are generally more favorable with fewer close-hauled conditions, D_M=1.1 is less cost-effective than D_M=2, as the positive aerodynamic interactions are less frequent and upwind penalties are higher. Furthermore, interaction penalties for Rotor Sails and DynaRigs are lower on the Atlantic route, making the impact of closely spaced devices less significant Figs. 4(a) and 4(b). Regarding unit count, DynaRigs and Rotor Sails exhibit opposite payback period trends under the IMO Wind Matrix route. DynaRigs see a decreasing payback period with more units, while Rotor Sails show the opposite trend. This divergence stems from two key factors. First, despite DynaRigs' better upwind performance, a single unit yields relatively low savings compared to its cost under this less favorable route, resulting in a higher payback period. However, installing multiple DynaRigs mitigates this effect, as aerodynamic penalties remain moderate, with even positive interactions Fig. 4(a), and economies of scale further reduce costs, lowering the payback period. In contrast, Rotor Sails experience stronger aerodynamic penalties in multi-unit setups due to their unique interactions Fig. 4(b), and a single unit already achieves a relatively low payback period—not due to higher savings, but due to lower cost. On the Atlantic route, where both WPS classes achieve higher savings, increasing the number of units leads to an increase in payback periods for both systems. Additionally, Fig. 13 highlights the impact of optimized versus non-optimized WPS installations, showing up to a 60% difference in payback period, underscoring the importance of installation optimization.

9.2.2. Full optimization

Next, WindWise is applied to optimize all configuration variables simultaneously—sail area, deck position, number of units, and relative mast spacing—for the same use case and WPS classes under study. This approach seeks to determine the optimal WPS configuration by considering all variables together, rather than optimizing them individually as done previously. Additionally, three optimizer constraints are imposed in the form of minimum emissions reduction targets of 10%, 25%, and 40%, aligned with the 2023 IMO GHG Strategy (MEPC, 2023). The results are presented in Fig. 14. Note that the optimization objective remains the same: minimizing the payback period.

Fig. 14(a) shows the minimum payback periods found by the optimizer, corresponding to the optimal WPS configurations for each WPS class, route, and minimum emissions reduction targets, as determined by WindWise. Notably, the optimization considers all configurations that meet or exceed the minimum fuel and emissions savings targets—not just those that precisely match the target. This means configurations achieving higher savings are also included if they result in a shorter payback period. The best WPS configurations for each scenario are presented in Table 6. The ideal configurations align with the trends observed in the previous parametric study.

The cost-efficiency analysis of Rotor Sails and DynaRigs reveals distinct trade-offs shaped by their aerodynamic properties, sensitivity to operating conditions, and cost dynamics Fig. 14. Rotor Sails generate higher thrust per square meter (see Fig. 11(b) for reference) but have a lower lift-to-drag ratio, leading to higher side forces per unit of thrust compared to DynaRigs. These side forces, increase yaw moments, which are also highly sensitive to deck placement Fig. 12, requiring significant rudder deflection and causing hydrodynamic penalties that reduce overall efficiency. Rotor Sails perform well and remain the most cost-effective under favorable side-wind conditions or at lower emissions targets, where reduced side forces or smaller installations keep hydrodynamic
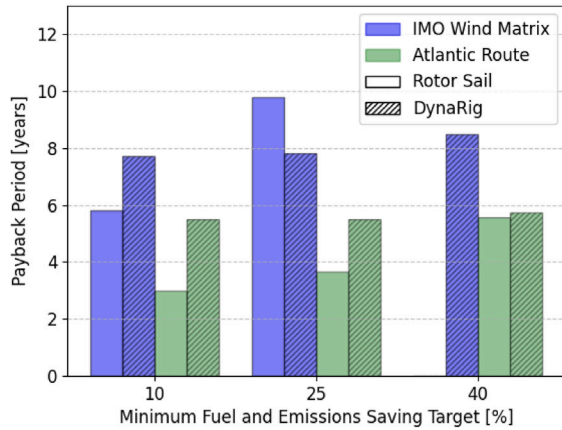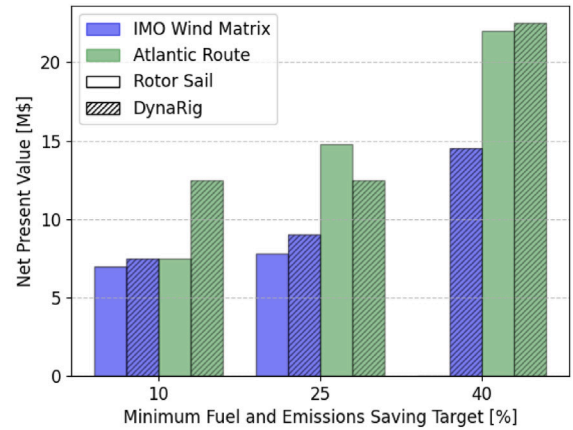
Fig. 14. Payback period and net present value calculations for the optimal WPS configurations across both WPS classes, route scenarios, and emissions reduction targets in the *Ideal* Scenario. The 40% savings target for Rotor Sails on the IMO route is not shown, as no studied configuration achieves this level of savings for the given route.

Fig. 15. Predicted fuel savings as a function of payback period and net present value for DynaRig configurations across both route scenarios.
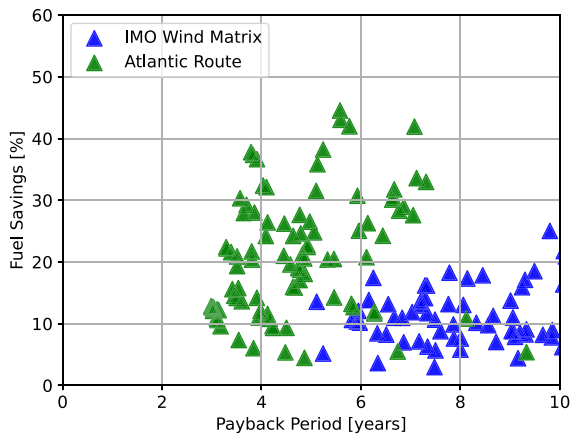
Fig. 16. Predicted fuel savings as a function of payback period and net present value for Rotor Sails configurations across both route scenarios.

Table 6

Most cost-effective WPS configuration for each WPS class and scenario under study found by WindWise. The 40% savings target for Rotor Sails on the IMO route is not shown, as no studied configuration achieves this level of savings for the given route.
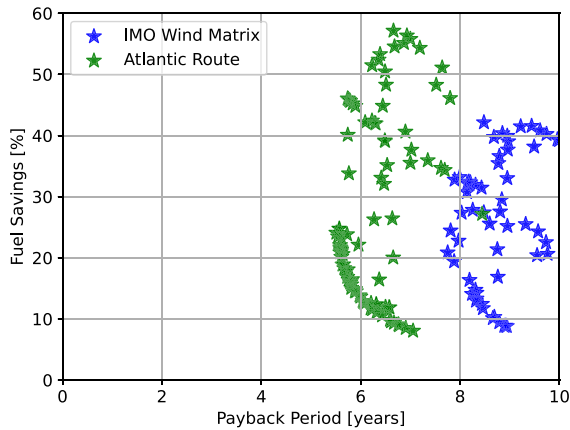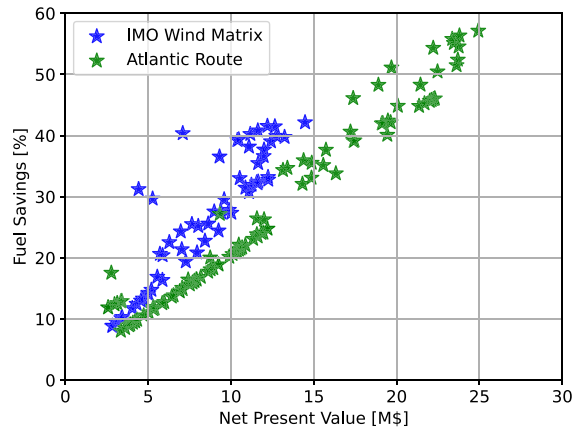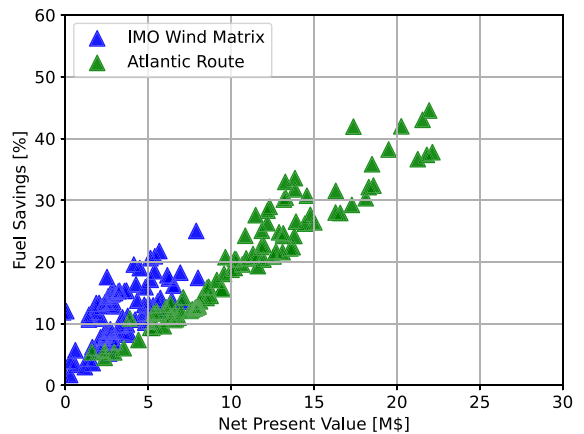
WPS class	Route	Min. Saving Target	Sail area	Number of units	Deck position	Mast spacing M_D
DynaRig	IMO	10%	1137 m^2	2	0.00	5.87
DynaRig	IMO	25%	1380 m^2	2	−0.02	4.69
DynaRig	IMO	40%	1807 m^2	3	−0.07	2.83
DynaRig	Atlantic	10%	1914 m^2	1	−0.22	–
DynaRig	Atlantic	25%	1914 m^2	1	−0.22	–
DynaRig	Atlantic	40%	2000 m^2	2	−0.10	3.79
Rotor Sail	IMO	10%	298 m^2	1	−0.16	–
Rotor Sail	IMO	25%	286 m^2	4	−0.11	5.20
Rotor Sail	IMO	40%	–	–	–	–
Rotor Sail	Atlantic	10%	199 m^2	1	0.00	–
Rotor Sail	Atlantic	25%	190 m^2	3	0.08	12.25
Rotor Sail	Atlantic	40%	259 m^2	5	−0.03	5.85

penalties manageable. However, at higher emissions targets, increasing side forces and hydrodynamic losses limit their effectiveness, particularly in close-hauled conditions. This is evident on the IMO Wind Matrix route, where no studied Rotor Sail configuration meets the 40% savings target Fig. 14(a). Beyond a certain installation size, additional Rotor Sails do not proportionally increase savings due to excessive hydrodynamic resistance counteracting the generated thrust (see Fig. 11(b) for reference). Incorporating underwater appendages or increased rudder area could mitigate these effects and enhance overall ship performance. However, such modifications would also lead to higher investment costs and increased baseline resistance. As this aspect falls outside the scope of the present study, it has not been explored further.

In contrast, DynaRigs, though producing less thrust per square meter Fig. 11(a), benefit from a higher lift-to-drag ratio, resulting in significantly lower side forces for the same thrust output, compared to Rotor Sails. This makes them more effective in close-hauled and close-reach conditions, where Rotor Sails face efficiency losses. As emissions targets increase and larger installations are required, DynaRigs maintain efficiency with lower hydrodynamic penalties and achieve all studied emissions savings targets without hull modifications. While their payback periods are longer at lower reduction targets than Rotor Sails, their ability to deliver higher absolute fuel and emissions savings at scale makes them the more cost-effective option for ambitious decarbonization goals, particularly under challenging wind conditions such as those on the IMO Wind Matrix route Fig. 14(a). Under the Atlantic Route, the threshold is surpassed at 45% of the minimum fuel and emissions savings target.

Focusing solely on payback period does not provide a complete understanding of the business case for each WPS class, despite existing literature relying solely on this metric for evaluation (Tillig and Ringsberg, 2020; Gerhardt et al., 2021). In terms of Net Present Value (NPV), as seen in Fig. 14(b), DynaRigs consistently outperform Rotor Sails across almost all scenarios. Despite Rotor Sails achieving shorter payback periods under most of the conditions under study, the superior fuel and emissions savings delivered by DynaRig ideal configurations result in higher NPV over the ship's lifetime, making them a more favorable business case for long-term operation. The exception is in scenarios with highly favorable winds for Rotor Sails, where their performance aligns more closely with DynaRigs, and their lower initial cost allows them to achieve similar savings. The differences between Payback periods and Net present values emphasize the importance of evaluating WPS installations beyond only payback period.

Finally, Figs. 15 and 16 illustrate fuel savings as a function of payback period and NPV, respectively, across all emissions reduction ambitions and route scenarios. A distinct Pareto trend emerges, highlighting the trade-offs between fuel savings, payback period, and NPV. This demonstrates that while different configurations can be optimal depending on the prioritization of specific objectives, no single configuration simultaneously optimizes all objectives universally.

9.3. Optimization scenario: Realistic

In this scenario, the maximum air draft is set to the Panamax size of 57.91 m above the waterline. The DynaRig reaches this maximum air draft at a total sail area of 925m^2, while the Rotor Sail reaches the limit at 400m^2, due to their different aspect ratios. Once the maximum air draft is reached, the WPS configuration is adjusted to include a tilting mechanism to comply with the requirement. This adjustment increases both the CAPEX and weight by 20%, as detailed in Section 7.

Additionally, the ship is assumed to be fully loaded while following the Atlantic Route under the Carbon Tax scenario. The cost of lost cargo space is accounted for based on a spot rate of $25 per ton of payload moved from origin to destination. As described in Lagouvardou et al. (2022), this rate represents an average for the given vessel and route. The Atlantic Route was selected due to the need for a specific spot rate, which varies by route. To estimate the maximum yearly impact, the case-specific route with the spot rate is analyzed under the assumption that the ship is fully loaded in both directions. With an average sailing time of 17 days per round trip and 280 operating days per year, the cost of lost cargo space totals approximately $411.76 per ton of payload annually.

Fig. 17 highlights the effects of incorporating payload reduction due to WPS weight and compliance with the maximum air draft limit. Compared to the *Ideal* scenario (in gray), where these constraints were not considered, both payback periods and net present values are impacted. Payback periods increase while net present values decrease for both WPS classes, reflecting the penalties associated with reduced payload and increased costs.
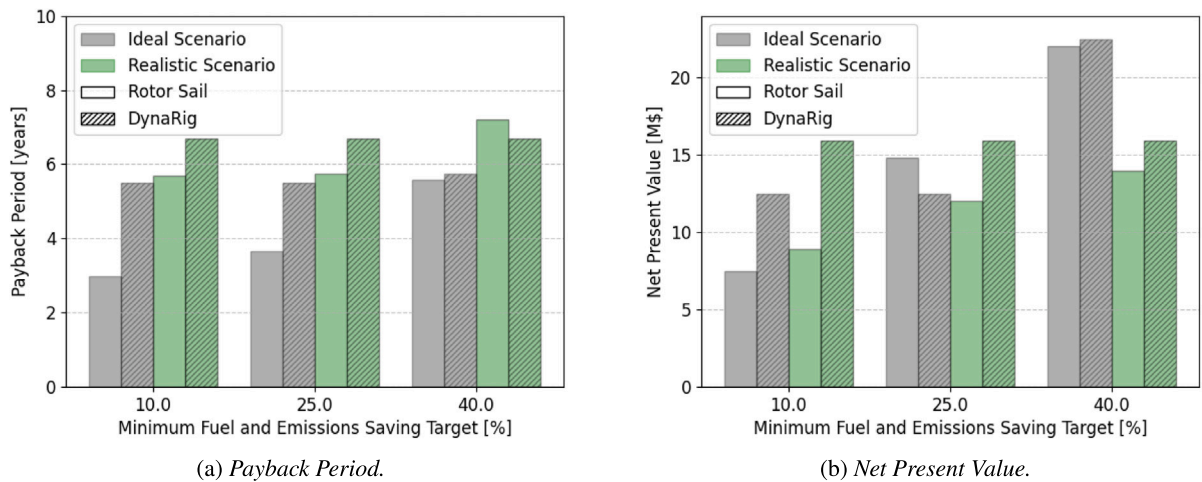
(a) *Payback Period.*

(b) *Net Present Value.*

Fig. 17. Payback period and net present value (NPV) calculations for the optimal WPS configurations identified across the Atlantic Route scenario, considering both WPS classes and three emissions reduction targets under the *Realistic* Scenario compared to the *Ideal* Scenario.
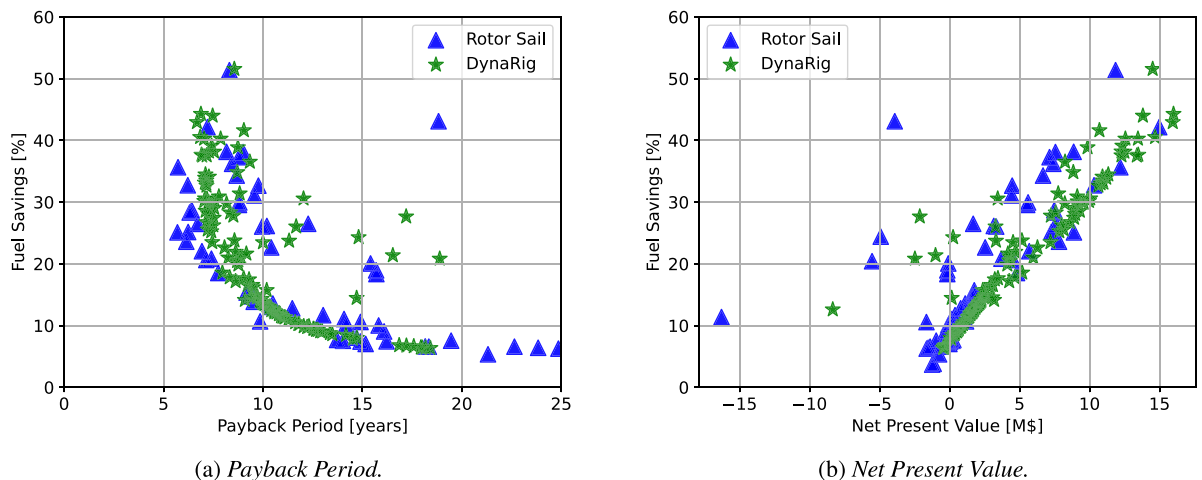

(a) *Payback Period.*

(b) *Net Present Value.*

Fig. 18. Predicted fuel savings as a function of payback period and net present value for Rotor Sails configurations across both route scenarios.

The analysis reveals a shift in cost-efficiency trends, particularly for Rotor Sails. While Rotor Sails were the most cost-effective option for all fuel and emissions savings targets on the Atlantic Route in the ideal scenario, they no longer maintain this status at the 40% savings target under the new constraints. At higher savings targets, DynaRigs become the more cost-effective solution due to their lightweight design and reduced sensitivity to payload penalties. This shift is partly attributed to the significant weight differences between the systems (see relative weights in Section 9.1). At lower reduction targets, the performance differences are less pronounced, as smaller installations of Rotor Sails are sufficient to meet the savings requirements. At lower reduction targets, the differences between the two systems are less pronounced, as smaller installations suffice for Rotor Sails.

Table 7 shows the ideal WPS configurations found for this new optimization scenario for both WPS classes and reduction targets. When comparing the ideal configurations from the initial scenario (see Table 6) to the configurations in this realistic scenario, notable changes are observed. Installations tend to be smaller in size (and therefore lighter) for both WPS classes, with a greater number of devices being used to achieve optimal performance. However, deck position and mast spacing trends remain consistent.

Despite the reduced net present values and increased payback periods, both WPS systems continue to deliver a positive business case. The impact of these constraints is more significant for Rotor Sails due to their overall sensitivity to weight penalties. DynaRigs, although requiring tiltable systems to meet air draft constraints, show more consistent performance across all targets, with the ideal WPS configuration being the same across all savings targets.

Finally, Fig. 18 illustrates fuel savings as a function of payback period Fig. 18(a) and NPV Fig. 18(b) across all emissions reduction targets for the Atlantic route scenario. As seen in Figs. 15 and 16, a clear Pareto trend emerges, emphasizing the trade-offs between fuel savings, payback period, and NPV. Despite the increase in overall payback periods and decrease in net present values, the key

Table 7

Most cost-effective WPS configuration for each WPS class and scenario under study found by WindWise.

WPS class	Route	Min. Saving Target	Sail area	Number of units	Deck position	Mast spacing M_D
DynaRig	Atlantic	10%	1200 m^2	3	0.00	3.80
DynaRig	Atlantic	25%	1200 m^2	3	0.00	3.80
DynaRig	Atlantic	40%	1200 m^2	3	0.00	3.80
Rotor Sail	Atlantic	10%	111 m^2	5	−0.06	6.98
Rotor Sail	Atlantic	25%	171 m^2	5	−0.06	6.25
Rotor Sail	Atlantic	40%	192 m^2	5	−0.01	5.56

distinction in this scenario is the emergence of certain WPS configurations with negative NPVs — due to weight-related penalties from WPS installations, leading to reduced payload capacity and increased costs — rendering them economically nonviable.

10. Conclusions

This study introduces WindWise, a cost–benefit analysis and design optimization tool for Wind Propulsion Systems (WPS) for sustainable shipping. Applied to a tanker retrofit case study, WindWise identifies the optimal configuration of Rotor Sails and DynaRigs across various emissions reduction targets, route scenarios, and fuel pricing conditions. Two optimization scenarios are analyzed: an ideal case with no constraints on air draft or cargo capacity and a realistic case that accounts for air draft limitations and lost cargo space due to WPS weight.

The results demonstrate that Rotor Sails and DynaRigs exhibit distinct aerodynamic and economic behaviors, with route conditions playing a critical role in their cost-effectiveness. Rotor Sails, with higher thrust per unit area, are more sensitive to deck placement and side forces, making them particularly suitable for side-wind routes and lower emissions reduction targets. However, their higher weight leads to a greater economic penalty when cargo space is reduced. In contrast, DynaRigs, benefiting from higher aerodynamic efficiency and lower side forces, become more cost-effective for higher emissions reduction targets and for routes with less favorable wind conditions. Generally, while Rotor Sails offer lower initial investment and shorter payback periods for smaller savings ambitions, DynaRigs prove to be the better option for greater fuel savings and fully wind-powered operations.

When realistic constraints are introduced, payback periods increase and net present values (NPV) decrease for both systems. The ideal WPS configurations differ significantly between the two scenarios. In the ideal case, both WPS classes benefit from larger, fewer, and well-spaced units to reduce aerodynamic interaction losses, which is particularly advantageous for routes with significant headwinds. In the realistic case, weight penalties shift the optimal design towards smaller installations with more units, mitigating the economic impact of cargo loss and air draft restrictions. Optimizing WPS installation—considering sail area, number of units, and deck placement—significantly enhances economic viability, with non-optimized configurations having payback periods over 150% higher than optimized ones. While payback period is a key indicator and the primary metric used in existing literature to evaluate the WPS business case, NPV provides a more comprehensive view of long-term financial performance. Although Rotor Sails often achieve shorter payback periods, they tend to result in lower NPV under demanding conditions, whereas DynaRigs demonstrate higher overall profitability across most scenarios.

These findings emphasize that no single WPS class universally outperforms the other, and case-specific evaluations are essential. Selecting the optimal WPS configuration requires a holistic assessment of route dynamics, ship and operational constraints, and long-term economic performance to unlock the full potential of wind propulsion in commercial shipping.

CRediT authorship contribution statement

M. Reche-Vilanova: Writing – review & editing, Writing – original draft, Visualization, Software, Methodology, Investigation, Funding acquisition, Formal analysis, Conceptualization. **H.B. Bingham:** Writing – review & editing, Supervision, Methodology, Funding acquisition, Conceptualization. **M. Fluck:** Writing – review & editing, Conceptualization. **D. Morris:** Writing – review & editing, Supervision, Project administration, Funding acquisition, Conceptualization. **H.N. Psaraftis:** Writing – review & editing, Methodology, Conceptualization.

Declaration of competing interest

The authors declare the following financial interests/personal relationships which may be considered as potential competing interests: Martina Reche-Vilanova reports financial support was provided by Innovation Fund Denmark. Martina Reche-Vilanova reports financial support was provided by The Danish Maritime Fund. If there are other authors, they declare that they have no known competing financial interests or personal relationships that could have appeared to influence the work reported in this paper.

Acknowledgments

References

Bertram, V., 2012. Practical Ship Hydrodynamics. Butterworth-Heinemann. Elsevier Ltd., UK.

Bonyadi, M.R., Michalewicz, Z., 2017. Particle swarm optimization for single objective continuous space problems: a review. Evol. Comput. 25 (1), 1–54.

Bordogna, G., 2020. Aerodynamics of Wind-Assisted Ships: Interaction Effects on the Aerodynamic Performance of Multiple Wind-Propulsion Systems (Ph.D. thesis). Delft University, Deflt, NL.

Bordogna, G., Muggiasca, S., Giappino, S., Belloli, M., Keuning, J., Huijsmans, R.H.M., 2020. The effects of the aerodynamic interaction on the performance of two Flettner rotors. J. Wind Eng. Ind. Aerodyn. 196, 104024.

Bradbury, W.M., 1980. An investigation of graduated trim for an aerofoil rig. In: Symposium on Wind Propulsion of Commercial Ships.

Carlton, J., 2018. Marine Propellers and Propulsion, second ed. Butterworth-Heinemann. Elsevier Ltd., UK.

Fakiolas, K.M., 2023. Empirical methods for developing WASP performance indicators and heuristics-based decision making under uncertainty. In: Wind Propulsion Conference 2023, London, UK.

Garzón, F., Figueroa, A., 2017. The study on the flow generated by an array of four Flettner rotors: theory and experiment. Appl. Math. 8 (12), 1851–1858.

Gerhardt, F., Werner, S., Hörteborn, A., Lundbäck, O., Nisbet, J., Olsson, T., 2021. Horses for courses: How to select the "right" wind propulsion system and how to make the business case. In: Wind Propulsion 2021, Online Conference.

Gunnarsson, H., Egilsson, J.L., 2024. A Numerical Study of Added Resistance from Leeway Caused by Wind Assisted Propulsion of Commercial Ships (Master's thesis). Technical University of Denmark, Lyngby, DK.

Hersbach, H., Bell, B., Berrisford, P., Hirahara, S., Horányi, A., Muñoz-Sabater, J., Nicolas, J., Peubey, C., Radu, R., Schepers, D., et al., 2020. The ERA5 global reanalysis. Q. J. R. Meteorol. Soc. 146 (730), 1999–2049.

Hollenbach, K.U., 1998. Estimating resistance and propulsion for single-screw and twin-screw ships-ship technology research 45 (1998). Schiffstechnik 45 (2), 72.

Hooft, J.P., 1994. The cross-flow drag on a manoeuvring ship. Ocean Eng. 21 (3), 329–342.

Houghton, E.L., Carpenter, P.W., 2003. Aerodynamics for Engineering Students. Butterworth-Heinemann. Elsevier Ltd., UK.

Hsu, S., Meindl, E.A., Gilhousen, D.B., 1994. Determining the power-law wind-profile exponent under near-neutral stability conditions at sea. J. Appl. Meteorol. Clim. 33 (6), 757–765.

IMO, 2022a. 2022 guidelines on operational carbon intensity indicators and the calculation methods (CII guidelines, G1). In: Resolution MEPC 78/17/Add. 1. MEPC. 352 (7). International Maritime Organization, London, UK.

IMO, 2022b. 2022 guidelines on operational carbon intensity rating of ships (CII rating guidelines, G4). In: Resolution MEPC 78/17/Add. 1. MEPC. 354 (78). International Maritime Organization, London, UK.

IMO, G., 2022c. 2022 guidelines on the reference lines for use with operational carbon intensity indicators (CII reference lines guidelines, G2). In: Resolution MEPC 78/17/Add. 1. MEPC. 353 (78). International Maritime Organization London, UK.

Inoue, S., Hirano, M., Kijima, K., Takashina, J., 1981. A practical calculation method of ship maneuvering motion. Int. Shipbuild. Prog. 28 (325), 207–222.

Kraft, D., 1988. A Software Package for Sequential Quadratic Programming. Wiss. Berichtswesen d. DFVLR, DE.

Kraft, D., 1994. Algorithm 733: TOMP–Fortran modules for optimal control calculations. ACM Trans. Math. Softw. (TOMS) 20 (3), 262–281.

Kume, K., Hasegawa, J., Tsukada, Y., Fujisawa, J., Fukasawa, R., Hinatsu, M., 2006. Measurements of hydrodynamic forces, surface pressure, and wake for obliquely towed tanker model and uncertainty analysis for CFD validation. J. Mar. Sci. Technol. 11, 65–75.

Lagouvardou, S., Psaraftis, H.N., Zis, T., 2022. Impacts of a bunker levy on decarbonizing shipping: a tanker case study. Transp. Res. Part D: Transp. Environ. 106, 103257.

Laursen, R., Patel, H., Sofiadi, D., Zhu, R., Nelissen, D., Van Seters, D., Pang, E., 2023. Potential of wind-assisted propulsion for shipping. In: European Maritime Safety Agency (EMSA) Report (EMSA/OP/43/2020). EMSA, Lisbon, Portugal, pp. 1–271.

MEPC, 2021. Guidance on Treatment of Innovative Energy Efficiency Technologies for Calculation and Verification of the Attained EEDI and EEXI. Technical Report, Technical Report MEPC. 1/Circ. 896, International Maritime Organization (IMO).

MEPC, 2023. 2023 IMO Strategy on Reduction of GHG Emissions from Ships. Technical Report, MEPC Resolution.

Nelissen, D., Traut, M., Koehler, J., Mao, W., Faber, J., Ahdour, S., 2016. Study on the analysis of market potentials and market barriers for wind propulsion technologies for ships. CE Delft.

Newman, J.N., 2018. Marine Hydrodynamics. The MIT press, Cambridge, USA.

Norsepower, 2023. English brochure. https://www.norsepower.com/technical-info/ [Brochure].

North Sails, 2019. Hull VPP & VPP. Technical Report, North Design Suite. [Confidential Document].

Prandtl, L., Betz, A., 1932. Ergebnisse der aerodynamischen Versuchsanstalt zu Göttingen. 4th version. Verlag von R. Oldenbourg, München, DE.

Rawson, K.J., Tupper, E.C., 2001. Basic Ship theory: Hydrostatics and Strength, vol. 1. Butterworth-Heinemann, UK.

Reche-Vilanova, M., Bingham, H.B., Fluck, M., Morris, D., Psaraftis, H.N., 2023. Optimal deck position of rotor sails and dynarigs for a bulk carrier retrofit installation. In: Sustainability in Ship Design and Operations Conference 2023, NY, USA.

Reche-Vilanova, M., Bingham, H.B., Fluck, M., Morris, H.N., 2024a. Propeller and engine performance of commercial windships: Benefits and trade-offs. J. Ship Res. 68 (01), 1–15.

Reche-Vilanova, M., Hansen, H., Bingham, H.B., 2021. Performance prediction program for wind-assisted cargo ships. J. Sail. Technol. 6, 91–117.

Reche-Vilanova, M., Kaltenbach, S., Koumoutsakos, P., Bingham, H.B., Fluck, M., Morris, D., Psaraftis, H.N., 2025. Predictive surrogates for aerodynamic performance and independent sail trim optimization of multiple wind propulsion system configurations. J. Sail. Technol. 10, 19–49.

Reche-Vilanova, M., Morris, D., Ward, H., Azcueta, R., Leslie-Miller, M., Bingham, H.B., 2024b. Development of machine-learning surrogates for hydrodynamic performance and wake-field prediction of windships. In: Wind Propulsion 2024, London, UK.

Schenzle, P., 1980. Standardised speed prediction for wind propelled merchant ships: Possible technologies and potential performance. In: Symposium on Wind Propulsion of Commercial Ships, London, UK.

Schenzle, P., 1985. Estimation of wind assistance potential. J. Wind Eng. Ind. Aerodyn. 20 (1), 97–110.

Schlichting, H., Gersten, K., 2016. Boundary-Layer Theory. Springer, USA.

Swanson, W.M., 1961. The Magnus effect: A summary of investigations to date. J. Basic Eng. 83 (3), 461–470.

Tillig, F., 2020. Simulation Model of a Ship's Energy Performance and Transportation Costs (Ph.D. thesis). Chalmers Tekniska Hogskola, Gothenburg, SE.

Tillig, F., Ringsberg, J.W., 2020. Design, operation and analysis of wind-assisted cargo ships. Ocean Eng. 211, 107603.

Van Brummelen, G., 2017. Heavenly Mathematics: The Forgotten Art of Spherical Trigonometry. Princeton University Press, Princeton, USA.

Van der Kolk, N., 2020. Sailing Efficiency and Course Keeping Ability of Wind Assisted Ships (Ph.D. thesis). Delft University, Deflt, NL.

Van der Kolk, N., Freeman, B., 2020. Machine learning based hydromechanics modelling for sailing commercial ships. In: Innov'sail, Virtual Conference.

Werner, S., 2022. Speed trial and route analysis of m/v Annika Braren with rotor sail. Interreg North Sea Region. No: RE40201042-03-00-A.

Zuhal, L.R., 2001. Formation and Near-Field Dynamics of a Wing Tip Vortex. California Institute of Technology, Pasadena, USA.